

# ROC curves for spatial point patterns and presence-absence data

Adrian Baddeley<sup>1</sup>, Ege Rubak<sup>2</sup>, Suman Rakshit<sup>3,4</sup>, and Gopalan Nair<sup>5</sup>

<sup>1</sup>*School of Population Health, Curtin University, Perth, Australia*

<sup>2</sup>*Department of Mathematical Sciences, Aalborg University, Aalborg, Denmark*

<sup>3</sup>*School of Electrical Engineering, Computing, and Mathematical Sciences, Curtin University, Perth, Australia*

<sup>4</sup>*Curtin Biometry and Data Analytics, Centre for Crop and Disease Management, Curtin University, Perth, Australia*

<sup>5</sup>*School of Mathematics & Statistics, University of Western Australia, Perth, Australia*

## Abstract

Receiver Operating Characteristic (ROC) curves have recently been used to evaluate the performance of models for spatial presence-absence or presence-only data. Applications include species distribution modelling and mineral prospectivity analysis. We clarify the interpretation of the ROC curve in this context. Contrary to statements in the literature, ROC does not measure goodness-of-fit of a spatial model, and its interpretation as a measure of predictive ability is weak; it is a measure of ranking ability, insensitive to the precise form of the model. To gain insight we draw connections between ROC and existing statistical techniques for spatial point pattern data. The area under the ROC curve (AUC) is related to hypothesis tests of the null hypothesis that the explanatory variables have no effect. The shape of the ROC curve has a diagnostic interpretation. This suggests several new techniques, which extend the scope of application of ROC curves for spatial data, to support variable selection and model selection, analysis of segregation between different types of points, adjustment for a baseline, and analysis of spatial case-control data. The new techniques are illustrated with several real example datasets. Open source R code implementing the techniques is available in the development version of our package `spatstat` [Baddeley and Turner, 2005, Baddeley et al., 2015] and will be included in the next public release.

## 1 Introduction

Receiver Operating Characteristic (ROC) curves have long been used to assess the performance of decision rules, classifiers and hypothesis tests [Krzanowski and Hand, 2009, Nam and D'Agostino, 2002]. The area under the ROC curve, AUC, provides a single numerical summary of performance, useful for comparing several competing tests or classifiers.

In recent decades, these tools have been used to evaluate the performance of models for spatial presence-absence and presence-only data in spatial ecology (species distribution models, Franklin, 2009) and in exploration geoscience (mineral prospectivity indices or mineral potential maps, Porwal et al., 2010, Fabbri and Chung, 2008, Ford et al., 2019, Khademi Zahedi, 2025). In these fields of application, the interpretation of ROC and AUC has been controversial. AUC is variously claimed to be a measure of *goodness-of-fit* of a predictive model [Fielding and Bell, 1997], a measure of *predictive power* [Lobo et al., 2007, Austin, 2007, Franklin, 2009] or a tool for *validation* of the model [Nykänen et al., 2015]. Some writers correctly warn that the ROC for spatial data depends on the choice of the spatial study domain [Jiménez-Valverde, 2012] and ignores the overall abundance or prevalence of the species [Manel et al., 2001].

The statistical interpretation of ROC curves for spatial data needs clarification. It is not necessarily valid to translate the original definition of the ROC curve (for classifying individuals in a population) into the context of spatial presence-absence data (for classifying pixels in a spatial grid) because pixels are not independent individuals. At the very least, the interpretation of ROC is different in the spatial context.

This article aims to clarify the interpretation of ROC and AUC for spatial presence-absence data, to identify their methodological strengths and weaknesses, and to develop improvements and extensions, including a new extension to spatial point pattern data.

In the literature on spatial data cited above, the term "ROC curve" refers exclusively to one particular form of the ROC curve, based on probabilities predicted by a model (which we call the "M-ROC"). In this paper we emphasise that many alternative applications of ROC curves are possible and useful for spatial data.

We find that the ROC and AUC for models of spatial presence-absence data do not measure goodness-of-fit of a predictive model. Rather, they measure "badness-of-fit" of the *null* model, i.e. the model in which the probability of

presence is the same at all locations. The M-ROC is the most optimistic of all variants of the ROC curve, is liable to the effects of over-fitting, and has poor ability to detect certain departures from the fitted model.

The interpretation of ROC and AUC as measures of predictive power is also weaker than generally believed. In the case of a single explanatory variable, ROC and AUC are almost completely unable to discriminate between different models or methodologies when applied to the same data; they only measure the ability of the *explanatory variable* to rank or segregate the study region into areas of high and low probability of presence. Furthermore, this ability to segregate space always refers to a specific region of space; the ROC and AUC can change markedly if we restrict attention to a sub-region of the original study region, or if we consider an adjacent spatial region, giving rise to instances of Simpson's Paradox. ROC curves cannot be used to predict behaviour on other spatial regions, or to predict the response to changes in covariate values (such as predicting the effect of climate change on a species range). Nevertheless, the fact that the M-ROC does not depend on the precise form of the model can be an advantage for some tasks such as variable selection.

To gain insight, we connect the ROC and AUC to other statistical techniques for spatial data, including hypothesis tests (Berman-Waller-Lawson, Kolmogorov-Smirnov), P-P plots (capture efficiency curve, fitting rate curve), and rate estimation (resource selection function, mineral prospectivity index, mineral potential map, continuous Boyce index, point process intensity). AUC is related to a test of the null hypothesis that the covariates have no effect, rather than a goodness-of-fit test. These connections improve understanding of the correct interpretation, statistical behaviour, and strengths and weaknesses of ROC and AUC, and help to identify conditions where they perform well. The strong connections also imply that these various techniques cannot be treated as independent pieces of corroborating evidence in favour of a model.

We develop new applications of the ROC and AUC to spatial presence-absence data. These new techniques support nonparametric analysis of dependence on a covariate, variable selection and model selection, analysis of segregation between different types of points, adjustment for a baseline, and analysis of spatial case-control data. We develop "fitted" and "theoretical" versions of the ROC curve for model validation. We provide variance formulae and strategies for avoiding overfitting. The new techniques are illustrated with several real example datasets. We discuss fields of potential application, including spatial ecology and geological prospectivity.

We also develop the ROC and AUC for *spatial point pattern* data, that is, data providing the exact spatial locations of the objects of interest. In geological prospectivity analysis, the primary survey data are the exact spatial coordinates of the mineral deposits, and these are usually discretised to obtain presence-absence data for analysis. This discretisation step is unnecessary: ROC and AUC can be calculated directly from the exact spatial coordinate data. Analysis based on the exact coordinates is often simpler than analysis based on discretised pixel data. These results also imply that ROC curves derived from presence-absence data using different choices of pixel size are consistent, asymptotically as pixel size tends to zero, because the limit is the spatial point pattern case. On the other hand the results also indicate that the ROC and AUC depend implicitly on the spatial coordinate system.

We find that the *shape* of the ROC curve has a diagnostic interpretation. Roughly speaking, if the ROC curve is concave or convex, then thresholding of the fitted probabilities is appropriate, and otherwise it is inappropriate.

The plan of the paper is as follows. Section 2 recalls the definition of ROC and AUC in a non-spatial context. Section 3 introduces spatial point pattern data, presence-absence data, spatial covariates, and parametric statistical modelling of point pattern and presence-absence data as a function of covariates. Section 4 develops the conceptually simplest application of the ROC curve to spatial presence-absence data and spatial point pattern data, for a single explanatory variable. This is not the most common version of the ROC curve but it gives clearer insight into strengths and weaknesses. Section 5 describes the "model ROC curve" that is typically used to assess the performance of a species distribution model or a mineral prospectivity index. It also investigates new kinds of ROC curves *predicted by* a species distribution model or prospectivity index. Section 6 shows that AUC and other measures of "performance" are related to tests of the null hypothesis that the explanatory variables have no effect, rather than tests of goodness-of-fit. In Section 7 we explain how to correctly "read" the ROC curve using its connection with the resource selection function (prospectivity index, intensity function). Section 8 develops new extensions of the ROC curve for spatial data, including ROC curves with non-uniform weights and non-uniform baselines, and applies them to model selection. Section 9 proposes new techniques for model checking, by comparing the empirical and model-predicted ROC curves, and by assessing convexity. We end with a Discussion in Section 10.

## 2 Background: ROC curves

Here we briefly recall the definition of ROC and AUC in a general context [Krzanowski and Hand, 2009].

## 2.1 ROC curve

Consider a classification rule or hypothesis test rule based on the value of a statistic  $S$ . An observation is allocated to the ‘Positive’ group (the null hypothesis is rejected) if  $S > t$ , and allocated to the ‘Negative’ group (the null hypothesis is Not rejected) if  $S \leq t$ , where  $t$  is a threshold value to be chosen. The probability of a true positive (the power of the test) is

$$\text{TP}(t) = \mathbb{P}\{S > t \mid \text{true status is Positive}\} \quad (1)$$

while the probability of a false positive (the size of the test) is

$$\text{FP}(t) = \mathbb{P}\{S > t \mid \text{true status is Negative}\}. \quad (2)$$

A good classifier is one which achieves a large value of  $\text{TP}(t)$  for any given value of  $\text{FP}(t)$ .

The ROC curve is loosely defined as a plot of  $\text{TP}(t)$  against  $\text{FP}(t)$  for all possible thresholds  $t$ . This may not define a continuous curve since  $\text{TP}$  and  $\text{FP}$  may be discontinuous; in that case it seems to be common practice to use a piecewise linear interpolant. We shall instead define the ROC curve as the graph of  $R(p)$  against  $p$  for all  $0 \leq p \leq 1$ , where

$$R(p) = \text{TP}(\text{FP}^{-1}(p)), \quad 0 \leq p \leq 1 \quad (3)$$

where  $\text{FP}^{-1}(p) = \max\{t : \text{FP}(t) \geq p\}$  is the left-continuous inverse function of  $\text{FP}$ . Then  $R(p)$  is a left-continuous, non-decreasing function of  $p$ . Good performance of the classifier is indicated by an ROC curve lying well above the diagonal line  $y = x$ .

In some applications it is appropriate to reverse the direction of thresholding, that is, to treat smaller values of  $S$  as more favorable to the Positive group. The classification rule allocates a subject to the Positive group if  $S \leq t$ . This “reversed ROC” curve will be denoted  $R^<(p)$ .

## 2.2 Empirical ROC from a finite dataset

Assume we observe data  $(s_1, y_1), \dots, (s_J, y_J)$  for  $J$  individuals, where  $s_j$  is the value of the statistic  $S$  for the  $j$ th individual and  $y_j$  is the indicator of true status, (i.e.  $y_j = 1$  if the  $j$ th individual truly belongs to the Positive group, and  $y_j = 0$  if Negative). The empirical ROC curve based on these data is the (interpolated) graph of the empirical true positive rate

$$\widehat{\text{TP}}(t) = \frac{\sum_{j=1}^J y_j \hat{y}_j}{\sum_{j=1}^J y_j} = \frac{\#\{j : y_j = 1, s_j > t\}}{\#\{j : y_j = 1\}} \quad (4)$$

against the empirical false positive rate.

$$\widehat{\text{FP}}(t) = \frac{\sum_{j=1}^J (1 - y_j) \hat{y}_j}{\sum_{j=1}^J (1 - y_j)} = \frac{\#\{j : y_j = 0, s_j > t\}}{\#\{j : y_j = 0\}}. \quad (5)$$

Equivalently, the empirical ROC curve is the plot of  $\widehat{R}(p) = \widehat{\text{TP}}(\widehat{\text{FP}}^{-1}(p))$  against  $p \in [0, 1]$ . This should not be conflated with the true (“theoretical”) ROC curve  $R(p)$  defined in (3).

Of course, (4) and (5) are not the only possible estimators of the functions  $\text{TP}$  and  $\text{FP}$ ; kernel estimates [Hall and Hyndman, 2003, Hall et al., 2004, Zou and Hall, 2000, Zou et al., 1997] are discussed in Section 4.3.2.

## 2.3 Measures of ‘performance’

When a single numerical value of ‘performance’ of a classifier is required, a popular choice is the area under the ROC curve,

$$\text{AUC} = \int_0^1 R(p) dp = \int_{-\infty}^{\infty} \text{TP}(t) d\text{FP}(t). \quad (6)$$

The last integral on the right hand side is a Stieltjes integral. Clearly  $0 \leq \text{AUC} \leq 1$ , and larger values of  $\text{AUC}$  are conventionally interpreted as implying greater discriminatory power. If the ROC falls on the diagonal line  $R(p) \equiv p$  then  $\text{AUC} = 1/2$ . Consequently, values of  $\text{AUC}$  close to  $1/2$  are interpreted as indicating a complete lack of discriminatory power. The area under the “reverse” ROC curve  $R^<(p)$  will be denoted  $\text{AUC}^<$  and satisfies  $\text{AUC}^< = 1 - \text{AUC}$ .

An alternative to AUC is the one-sided Youden criterion (Youden, 1950, Krzanowski and Hand, 2009, p. 30) defined as the greatest positive deviation of the ROC curve above the diagonal,

$$J = \max_t (\text{TP}(t) - \text{FP}(t))_+ = \max_p (R(p) - p)_+ \quad (7)$$

where  $x_+ = \max(0, x)$  denotes the positive part. This originated in medical diagnostics and has been used in mineral prospectivity analysis [Ruopp et al., 2008, Chen and Wu, 2019, Baddeley et al., 2021, Khademi Zahedi, 2025].

## 2.4 Relation of ROC to comparison of probability distributions

The ROC curve is closely related to the *P–P plot* [Wilk and Gnanadesikan, 1968], a standard tool for comparing two probability distributions. While the ROC curve is usually conceived as a comparison between the *disjoint* populations of positive and negative individuals, the P–P plot is a comparison between any two probability distributions, including distributions in overlapping populations.

Consider two random variables  $X$  and  $Y$  with cumulative distribution functions  $F_X(t) = \mathbb{P}\{X \leq t\}$  and  $F_Y(t) = \mathbb{P}\{Y \leq t\}$ . The P–P plot is a plot of  $F_Y(t)$  against  $F_X(t)$  for all  $t$ , or equivalently, the graph of  $H(p)$  against  $p$  for  $0 \leq p \leq 1$ , where

$$H(p) = F_Y(F_X^{-1}(p)), \quad (8)$$

where  $F_X^{-1}(p) = \inf\{x : F_X(x) \geq p\}$  is the right-continuous inverse function of  $F_X$ .

In the context of ROC curves, let  $S_P$  and  $S_N$  be random variables denoting the discriminant scores for randomly selected members of the positive and negative groups respectively. These random variables have cumulative distribution functions  $F_P(t) = 1 - \text{TP}(t)$  and  $F_N(t) = 1 - \text{FP}(t)$ . Accordingly, the ROC curve is

$$R(p) = \text{TP}(\text{FP}^{-1}(p)) = 1 - F_P(F_N^{-1}(1 - p)), \quad 0 \leq p \leq 1. \quad (9)$$

and conversely the P–P plot is the “reversed” ROC curve

$$R^<(p) = F_P(F_N^{-1}(p)) = 1 - \text{TP}(\text{FP}^{-1}(1 - p)), \quad 0 \leq p \leq 1 \quad (10)$$

so that  $R^<(p) = 1 - R(1 - p)$ . That is, the P–P plot and ROC curve are equivalent when the axes are reversed.

## 2.5 Probability integral transformation

The connection to P–P plots shows that ROC curves are related to the probability integral transformation. If the distributions of  $S_N$  and  $S_P$  are continuous, for example, then  $R^<(p)$  is the cumulative distribution function

$$R^<(p) = \mathbb{P}\{F_N(S_P) \leq p\} \quad (11)$$

of the values  $U = F_N(S_P)$ , and similarly

$$R(p) = \mathbb{P}\{F_N(S_P) \geq 1 - p\} = \mathbb{P}\{1 - F_N(S_P) \leq p\} \quad (12)$$

is the c.d.f. of the values  $V = 1 - F_N(S_P)$ . If the distributions of  $S_N$  and  $S_P$  were identical (and continuous) then  $U$  and  $V$  would be uniformly distributed between 0 and 1.

From this it can be derived that AUC has the elegant interpretation

$$\text{AUC} = \mathbb{P}\{S_P > S_N\} \quad (13)$$

where  $S_P$  and  $S_N$  are values of  $S$  for independent, randomly-selected members of the Positive and Negative groups, respectively. We also have  $\text{AUC} = \mathbb{E}[U] = 1 - \mathbb{E}[V]$ .

## 3 Background: spatial data and models

We are concerned with the spatial distribution of ‘individuals’, which may be individual animals or organisms of a particular species, or mineral deposits of a particular kind. We assume the individuals have negligible size at the scale of interest. The original observations may be either a list of the exact spatial coordinates of the observed individuals, or an array of binary variables indicating the presence or absence of individuals in the cells of a grid.

### 3.1 Spatial point pattern

In a “mapped” spatial point pattern [Diggle, 1983, 2014, Ripley, 1981, Cressie, 1991, Illian et al., 2008, Baddeley et al., 2015] the available data are the exact spatial locations of the individuals observed within a given sampling region  $W \subset \mathbb{R}^d$ . The point pattern is a finite set  $\mathbf{x} = \{x_1, \dots, x_n\}$ ,  $n \geq 0$ ,  $x_i \in W$  where the number of points  $n$  is not fixed in advance. It will be assumed that two individuals cannot exist at the same location.

The left panel of Figure 1 shows a typical mapped point pattern dataset giving the locations of 3604 trees of the species *Beilschmiedia pendula* (Lauraceae) in a 1000-by-500 metre rectangular sampling region in the tropical rainforest of Barro Colorado Island [Hubbell and Foster, 1983, Condit et al., 1996, Condit, 1998].

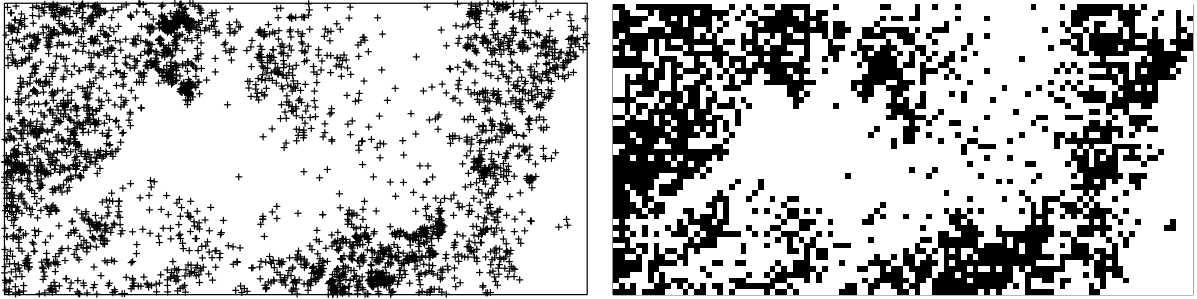


Figure 1: *Beilschmiedia* tree data. *Left*: Exact tree locations (+) in a 1000 by 500 metre survey region. *Right*: Presence-absence indicators for a grid of 10-metre square pixels. Black indicates presence.

### 3.2 Presence-only and presence-absence data

In “presence-only” and “presence-absence” data [Franklin, 2009] the study region is subdivided into cells. In each cell, individuals may be either “present” (observed to be present in the cell), “absent” (determined to be absent from the cell) or “undetermined” (not conclusively determined to be either present or absent). Presence-absence data record “presence” or “absence”, for those cells whose status is known. Presence-only data record “presence” or “non-presence” (absence or undetermined status) for every cell in the study region.

Assume the study region  $W$  is partitioned into cells  $Q_1, \dots, Q_J$  of equal area  $a$ . For each cell  $Q_j$  (or for a subset of cells for which observations are available) let  $y_j$  be the *presence indicator* that equals 1 if the cell  $Q_j$  is observed to contain any individuals of the species (“presence”) and 0 otherwise (implying “absence” for presence-absence data; “absence” or “unknown” for presence-only data). The data consist of the vector of indicator variables  $\mathbf{y} = (y_1 \ y_2 \ \dots \ y_J)^\top$ .

A mapped point pattern  $\mathbf{x}$  can be discretised to obtain presence-absence data. Let  $n_j = n(\mathbf{x} \cap Q_j)$  denote the number of points of the observed point pattern  $\mathbf{x}$  that fall inside the  $j$ th cell. Then  $y_j = \mathbf{1}\{n_j > 0\}$  takes the value 1 if the  $j$ th cell contains any points of  $\mathbf{x}$ , and 0 if it does not.

The right panel of Figure 1 shows indicators of presence or absence of *Beilschmiedia pendula* trees in a grid of 10-metre-square pixels superimposed on the previous Figure. In this illustrative example, the presence-absence data were derived by discretising the exact coordinate data shown in the left panel of Figure 1 as described above.

In ecological applications the exact coordinates are typically not recorded, and the presence-absence or presence-only data are the original observations; while in many applications to geological prospectivity, exact coordinates are indeed discretised to produce pixel-based presence-absence data for further analysis.

In the right panel of Figure 1 there are 1753 pixels in which *B. pendula* is present, while 3604 trees are depicted in the left panel.

### 3.3 Multitype point patterns and case-control data

A “multitype” point pattern is a mapped spatial point pattern in which each point is labelled as belonging to one of several different types. Examples include survey maps of trees in a forest labelled by species, catalogues of galaxies labelled by type or colour, and microscope images of cell populations labelled by cell type. In spatial case-control data in epidemiology, there are two types of points which represent respectively disease cases and (a sample from) the population at risk [Jarner et al., 2002, Diggle et al., 2007].

Figure 2 shows the locations of centres of cell profiles in a histological section of the gastric mucosa (mucous membrane of the stomach) of a rat. The window is oriented so that the lower edge is closest to the stomach wall while the upper edge is interior to the stomach. The cells are classified into two types: there are 86 *ECL cells* (enterochromaffin-like cells) and 807 *other cells*. The intensities of each type of cell are clearly non-uniform. One hypothesis of interest is whether the ratio of ECL cells to other cells is constant over the region; equivalently, whether the spatially-varying intensities of ECL cells and other cells are proportional. An alternative hypothesis is that ECL cells are relatively more abundant at locations close to the stomach wall. The data were originally collected by Dr Thomas Berntsen, and have been discussed and analysed in Møller and Waagepetersen [2004, pp. 2, 169].

### 3.4 Spatial covariates

A spatial covariate (or “evidence layer”) is a real-valued function  $Z(u), u \in W$  defined on the study region. Examples in geological science include isotope abundance ratio, magnetic field strength, and terrain slope.

Figure 3 shows contour maps of two spatial covariates, terrain elevation and terrain slope, which are available for the survey region of the *Beilschmiedia pendula* data.

The left panel of Figure 4 shows data from a geological survey of the Murchison region in Western Australia [Watkins and Hickman, 1990] first analysed by Knox-Robinson and Groves [1997]. Crosses indicate the locations of known gold deposits. Lines represent geological faults, and grey-shaded polygons represent a particular rock type, greenstone outcrop. The main aim is to predict the spatially-varying abundance of gold deposits from the more easily observable fault pattern and the greenstone outcrop map. Figure 4 strongly suggests that proximity to faults is predictive for gold prospectivity.

The covariate information consists of the greenstone region and the geological faults. For modelling purposes these must be converted to spatial functions  $Z(u)$ ,  $u \in W$ . For the geological fault lines, a common choice is the *distance function*  $D(u)$  defined for any location  $u$  as the shortest distance from  $u$  to the nearest geological fault [Knox-Robinson and Groves, 1997, Baddeley, 2018]. The right panel of Figure 4 shows contours of this function. For the greenstone polygons, the indicator function defined by  $G(u) = 1$  if location  $u$  lies inside the greenstone and  $G(u) = 0$  otherwise, will be used in some of our examples.

### 3.5 Models for spatial data which depend on covariates

#### 3.5.1 Presence-absence data

To investigate whether the *B. pendula* trees exhibit a preference for higher terrain elevation (for example), a standard approach using the presence-absence data is to fit a logistic regression model for the probability of presence as a function of terrain elevation,

$$\log \frac{\pi_j}{1 - \pi_j} = \log a + \beta_0 + \beta_1 Z_j \quad (14)$$

where, for a given pixel  $Q_j$ , the probability of presence of the species is  $\pi_j$ , and  $Z_j$  is the terrain elevation. Here  $\beta_0, \beta_1$  are parameters to be estimated, and the offset  $\log a$  (where  $a$  is pixel area) ensures comparability of results obtained using different pixel sizes. This approach was developed independently by Lewis [1972], Tukey [1972], Agterberg [1974], Brillinger [1978], Kvamme [1983] and others. See Baddeley [2018] for a recent survey.

A surprising common misconception in the applied literature is that logistic regression is a nonparametric technique [Kvamme, 2006, p. 24], i.e. that it does not assume any particular form of the relationship between  $p$  and  $Z$ . On the contrary, the logistic regression equation (14) specifies a linear relationship between the predictor  $Z$  and the log odds of presence. A truly nonparametric model would take the form

$$\frac{\pi_j}{1 - \pi_j} = a\rho(Z_j) \quad (15)$$

where  $\rho(z)$  is an unknown function to be estimated. This model, and its important connections with ROC curves, will be discussed in Section 7. In real applications, the model typically involves several explanatory variables, so that in the equations above,  $Z_j$  and  $Z(u)$  may be  $m$ -dimensional vectors representing the values of  $m$  scalar valued covariates.

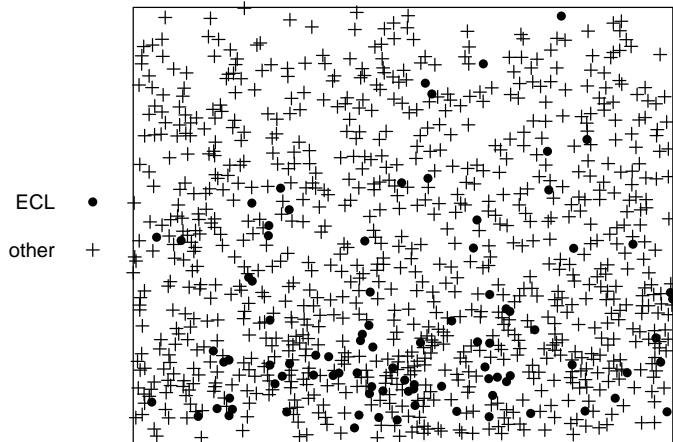


Figure 2: Gastric mucosa data, showing locations of enterochromaffin-like cells (•) and other cells (+). Lower edge is closest to stomach wall. Collected by Dr Thomas Berntsen.

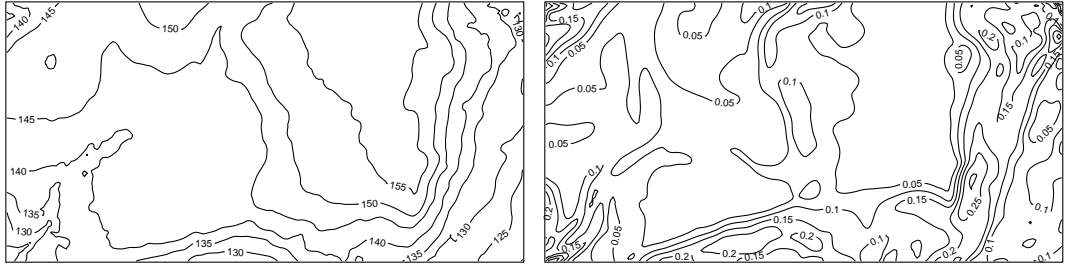


Figure 3: Contours of terrain elevation in metres (Left) and contours of terrain slope (Right) for the *Beilschmiedia pendula* data.

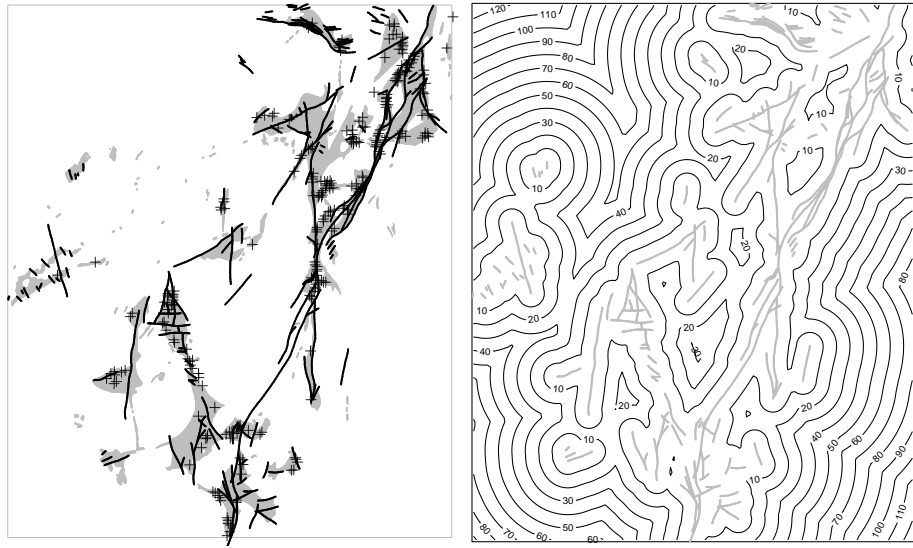


Figure 4: Murchison data. *Left*: gold deposits (+), geological faults (—) and greenstone outcrop (grey shading) in a survey region 330 by 400 kilometres across. Vector (spatial coordinate) data, rounded to the nearest metre. *Right*: Contours of distance (in km) to the nearest geological fault in the Murchison data. Faults shown as light grey lines.

### 3.5.2 Mapped spatial point patterns

For mapped point patterns, the corresponding approach is to fit a Poisson point process model in which the point process intensity is a loglinear function of the covariate. The observed point pattern  $x$  is assumed to be a realisation of a Poisson point process  $\mathbf{X}$  in  $W$ , with intensity (expected number of points per unit area)

$$\log \lambda(u) = \beta_0 + \beta_1 Z(u), \quad u \in W \quad (16)$$

at any given spatial location  $u \in W$ , where  $Z(u)$  is the covariate. The close connection between the logistic regression and the Poisson point process model is explained by Baddeley et al. [2010], Warton and Shepherd [2010]. The logistic regression model (14) is asymptotically equivalent to the loglinear Poisson model (16) for small pixel size.

Again, the loglinear relationship (16) is a simplifying model assumption, which may be false in a real application. A nonparametric model would take the form

$$\lambda(u) = \rho(Z(u)), \quad u \in W, \quad (17)$$

where  $\rho$  is a function to be estimated. Again we shall find that  $\rho$  is closely related to the ROC curve.

### 3.5.3 Interpretation of models

A properly-formulated species distribution model (SDM) or binary regression or point process model is a kind of “law” expressing species’ preference for particular habitat, etc. and can conceivably be extrapolated from one study region to another.

In principle, such a model predicts the abundance of data points at any given location where covariate values are known. However, in many applications to spatial data, the main goal of modelling is to identify the conditions which *maximise* the abundance of data points. In ecology, attention is often focused on the “home range” or “favorable conditions” for a species. Models are used in order to understand species requirements, manage species, predict change (e.g. response to climate change), and assess risks. Covariates are chosen for their explanatory power in a model [Elith and Leathwick, 2009]. In exploration geology, the goal is to identify the *highest* spatial concentration of mineral deposits, and there is no interest whatsoever in modelling the lack of deposits in non-prospective places. Covariates may be chosen for operational reasons rather than for scientific understanding [Ford et al., 2019].

This paper does not make assumptions about the particular models (such as species distribution models, logistic regressions and point process models) or predictive procedures (such as machine learning [Yeomans, 2018] or fuzzy predictors [Zhang and Zhou, 2015]) that may be in use. It applies to the use of ROC and AUC for evaluating the performance of all such models and predictive procedures.

### 3.5.4 Spatial case-control data

A spatial case-control point pattern can be analysed with or without conditioning on the observed locations [Diggle, 1990, Diggle and Rowlingson, 1994]. In the unconditional analysis, the data are treated as a realisation of a bivariate spatial point process, requiring a model for the random spatial locations of the points. The spatial relative risk (the spatially-varying probability of a case) is determined by the ratio of the intensities of cases and controls. In the conditional analysis, the locations  $x_i$  are treated as fixed, and the type labels  $m_i$  (where  $m_i = 1$  denotes a case and  $m_i = 0$  denotes a control) are modelled as a realisation of a binary random field at the sites  $x_i$ . The spatially-varying relative risk at a location  $x_i$  is the probability that  $m_i = 1$ . When the analysis includes covariates, an advantage of the conditional analysis is that the values of the covariates are required only at the locations  $x_i$ .

In this article we assume that the analysis of case-control data is conditional on the locations. Thus, we have  $J$  irregularly placed spatial locations  $x_j$ ,  $j = 1, \dots, J$  where we model the conditional probability of the point at location  $x_j$  being a case,  $\pi_j = P(m_j = 1)$ . This model may be directly specified (e.g. as having the same form as the pixel based model in (14)), or it may be derived from an underlying point process model assumed to have generated the marked point pattern; see Baddeley et al. [2015, pp. 358–359]; Diggle [1990], Diggle and Rowlingson [1994].

## 4 ROC for a spatial covariate

The ROC curve is often regarded as a tool for assessing the performance of a model. However, it is possible to construct an ROC curve without involving a model, using only the raw data (spatial point pattern or presence-absence data) and using any spatial covariate as the discriminant variable. We call this the “covariate ROC” (C-ROC) and describe it below.

Many aspects of ROC curves are easier to understand and explain in this context where the discriminant is a fixed covariate, than in the more complicated case where the discriminant is derived from a fitted model. Many of the conclusions of this section also apply to the “model ROC” discussed in subsequent sections.

### 4.1 Definition

Assume there is a single, given, real-valued spatial covariate  $Z$ , which may be one of the original explanatory variables, or may have been constructed from them, e.g. the distance to the nearest fault line in the Murchison example of Section 3.4. The objective is to assess whether  $Z$  has utility for predicting the abundance and distribution of points, without assuming any specific model for the dependence on  $Z$ . In applications, the use of a single covariate may be an initial or interim step in an analysis involving many explanatory variables.

#### 4.1.1 Presence-absence data

In the case of presence-absence data (Section 3.2), the data consist of the presence indicators  $y_j$  for pixels  $Q_j$ ,  $j = 1, \dots, J$ . For any given threshold  $t \in \mathbb{R}$ , consider the classifier  $\hat{y}_j = \mathbf{1}\{z_j > t\}$ . The empirical C-ROC curve is defined as the empirical ROC curve (Section 2.2) based on these data. The spatial covariate  $Z$  plays the role of the statistic  $S$  in equations (4) and (5), and the empirical C-ROC curve is the graph of  $\widehat{\text{TP}}(t)$  against  $\widehat{\text{FP}}(t)$ , where

$$\widehat{\text{TP}}(t) = \frac{\#\{j : y_j = 1, z_j > t\}}{\#\{j : y_j = 1\}}, \quad \widehat{\text{FP}}(t) = \frac{\#\{j : y_j = 0, z_j > t\}}{\#\{j : y_j = 0\}} \quad (18)$$

This empirical version of the C-ROC curve will be denoted  $R_{Z,y}(p)$  where  $y = (y_1, \dots, y_J)$  is the vector of presence indicators.

This version of the ROC curve is based solely on a spatial covariate, without reference to a model. It has been used at least once in mineral prospectivity analysis [Goodacre et al., 1993] but we have not found other references.

In (18) we note that  $\widehat{\text{TP}}$  is computed from the observed data at ‘presence’ pixels and  $\widehat{\text{FP}}$  from ‘absence’ pixels. This is consistent with the implicit assumption in Section 2 that the Positive and Negative populations are disjoint. However, in the spatial context, where the status of each pixel can be either positive or negative (presence or absence), it might be more appropriate to replace  $\widehat{\text{FP}}(t)$  in (18) by

$$\widetilde{\text{FP}}(t) = \frac{1}{J} \sum_j \hat{y}_j = \frac{1}{J} \sum_j \mathbf{1}\{z_j > t\} \quad (19)$$

the fraction of *all* pixels that are predicted to contain a presence. This is simpler to interpret, since it is the fraction of area in the survey region where the covariate value  $z_j$  exceeds the nominated threshold  $t$ . The discrepancy between  $\widehat{\text{FP}}(t)$  and  $\widetilde{\text{FP}}(t)$  is small when pixel size is small. In applications to mineral prospectivity, this approach is useful because it avoids the difficult task of finding “true negative” pixels [Nykänen et al., 2015].

Under suitable conditions the empirical true positive rate  $\widehat{\text{TP}}(t)$  in (18) is a pointwise consistent estimator of the “true” rate of true positives

$$\text{TP}(t) = \frac{\sum_{j=1}^J \pi_j \mathbf{1}\{z_j > t\}}{\sum_{j=1}^J \pi_j}, \quad (20)$$

where  $\pi_j$  is the (unknown) true probability that pixel  $j$  contains a presence. Similarly, the empirical false positive rate  $\widehat{\text{FP}}(t)$  in (18) and the alternative version  $\widetilde{\text{FP}}(t)$  in (19) are both pointwise consistent estimators of the true rate of false positives

$$\text{FP}(t) = \frac{\sum_{j=1}^J (1 - \pi_j) \mathbf{1}\{z_j > t\}}{\sum_{j=1}^J (1 - \pi_j)}. \quad (21)$$

A plot of (20) against (21) shall be called the “true” or “theoretical” C-ROC curve for the covariate  $Z$ , and denoted  $R_{Z,\pi}(p)$  where  $\pi = (\pi_1, \dots, \pi_J)$  is the vector of presence probabilities.

For a fitted model with estimated presence probabilities  $\hat{\pi}_j$  the “model-predicted” C-ROC curve,  $R_{Z,\hat{\pi}}$  is defined similarly, with  $\pi$  replaced by  $\hat{\pi}$  in (20) and (21).

The calculations above treat every pixel as having equal weight, and could be inappropriate in applications where pixels do not have equal area. Examples include geographical projections of observations on the Earth’s surface where the projection does not have unit Jacobian, such as the projection to latitude-longitude coordinates. Appropriate adjustments to the C-ROC curve are described in Section 8.3.

#### 4.1.2 Spatial point pattern data

In the case of mapped spatial point pattern data (Section 3.1), the data consist of the exact coordinates of the observed points,  $x = \{x_1, \dots, x_n\}$ . The continuous-space counterpart of  $\widehat{\text{TP}}(t)$  in (18) is

$$\widehat{\text{TP}}(t) = \frac{1}{n} \sum_{i=1}^n \mathbf{1}\{Z(x_i) > t\}, \quad (22)$$

the fraction of data points  $x_i$  at which the covariate value  $Z(x_i)$  exceeds the threshold. Equivalently,  $1 - \widehat{\text{TP}}(t)$  is the c.d.f. of the covariate value  $Z(x_I)$  at a randomly-selected data point  $x_I$  (where  $I$  is uniformly distributed on  $\{1, 2, \dots, n\}$ ). The continuous-space counterpart of both  $\widehat{\text{FP}}(t)$  in (18) and  $\widetilde{\text{FP}}(t)$  in (19) is

$$\widehat{\text{FP}}(t) = \frac{1}{|W|} \int_W \mathbf{1}\{Z(u) > t\} du, \quad (23)$$

the fraction of *area* in the study region where the covariate value exceeds the threshold. Here  $|W|$  is the area of the study region  $W$ . Equivalently,  $1 - \widehat{\text{FP}}(t)$  is the c.d.f. of the covariate value  $Z(U)$  at a random location  $U$  uniformly distributed in  $W$ . The graph of  $\widehat{\text{TP}}(t)$  against  $\widehat{\text{FP}}(t)$  is the empirical C-ROC curve  $R_{Z,x}(p)$ .

The continuous space versions (22)–(23) can be derived as the limit of the discrete versions (18) for the presence-absence case as the pixel size  $a$  tends to zero, under regularity assumptions on the covariate  $Z$ , and assuming all points  $x_i$  are distinct. The alternative form (19) also converges to (23).

The continuous-space version of the C-ROC curve (22)–(23) resolves issues inherent in the presence-absence case, about the choice of pixel size, and the loss of information due to discretisation. It can be used to establish connections with other methodology for spatial point patterns.

Under suitable conditions, the empirical true positive rate  $\widehat{\text{TP}}(t)$  in (22) is a consistent estimator of the “true” or “theoretical” true positive rate

$$\text{TP}(t) = \frac{\int_W \mathbf{1}\{Z(u) > t\} \lambda(u) du}{\int_W \lambda(u) du} \quad (24)$$

where  $\lambda(x)$  is the intensity function of the point process  $\mathbf{X}$ . The empirical false positive rate (23) is non-random and can be treated as the “true” or “theoretical” false positive rate  $\text{FP}(t)$ . The graph of  $\text{TP}(t)$  against  $\text{FP}(t)$  is the “theoretical” C-ROC curve  $R_{Z,\lambda}(p)$  for the point process  $\mathbf{X}$ .

For a point process model with fitted intensity  $\widehat{\lambda}(x)$  the “model-predicted” C-ROC curve,  $R_{Z,\widehat{\lambda}}(p)$  is defined similarly, with  $\lambda$  replaced by  $\widehat{\lambda}$  in (24) (and  $\text{FP}(t)$  unchanged).

#### 4.1.3 Case-control data

For spatial case-control data, it is straightforward to define the C-ROC of a spatial covariate  $S$ . The point patterns of cases and controls are combined into a single pattern of points numbered  $1, \dots, J$ ; the indicator variable  $y_j$  equals 1 if point  $j$  is a disease case, and 0 if it is a control; then the ROC is based on (4)–(5), effectively treating the cases and controls as samples from the positive and negative populations, respectively. The true positive rate (4) is the fraction of disease cases where  $S > t$ ; the false positive rate (5) is the fraction of controls where  $S > t$ . The ROC curve is the reverse P–P plot of the distributions of  $S$  in the cases and the controls. The case-control ROC will be denoted  $R_{S,x,y}(p)$  where  $x$  and  $y$  are the point patterns of cases and controls respectively. The technique can be used to investigate “relative risk” in spatial epidemiology [Bithell, 1991, Diggle and Rowlingson, 1994, Hazelton and Davies, 2009] and “segregation” of different types of points [Dixon, 1994, Diggle et al., 2005].

## 4.2 Examples

Here we compute C-ROC curves for the example datasets introduced in Section 3.

#### 4.2.1 *Beilschmiedia* trees

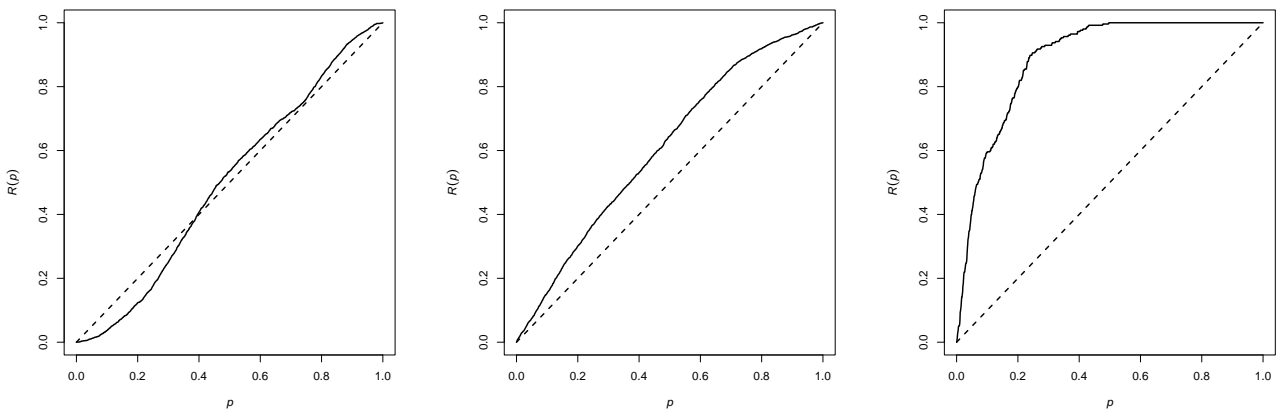


Figure 5: *Left and middle*: Empirical C-ROC curves computed for the *Beilschmiedia* data using the presence-absence indicators in 10-metre pixels treating higher values of the covariate as favorable to trees where the covariate is either terrain elevation (*Left*) or terrain slope (*Middle*). *Right*: Empirical C-ROC curve based on the distance  $D(u)$  to the nearest geological fault for the Murchison gold data, interpreting short distances as more favorable to gold.

The left and middle panel of Figure 5 shows the empirical C-ROC curves for terrain elevation and terrain slope in the *Beilschmiedia* data (Figure 3), computed from the presence-absence indicators in 10-metre pixels (right panel

of Figure 1), treating higher elevations and steeper slopes as more favorable to the *Beilschmiedia* trees. The curve for terrain elevation has an ‘S’ shape and the computed AUC is 0.51, suggesting a weak or inconsistent association between elevation and tree abundance. The curve for terrain slope is a more satisfactory convex curve with AUC equal to 0.61, suggesting that steeper slopes are slightly more favorable to trees. However, using the approach described in Section 7, a more accurate explanation is that very flat areas are relatively unfavorable, while all other slopes are equally favorable. Flat areas include watercourses and swamps which would not be expected to support trees. This suggests that there is no evidence of a preference for particular terrain slopes.

#### 4.2.2 Murchison gold data

The right panel of Figure 5 shows the empirical C-ROC curve  $\hat{R}_{D,x}^<(p)$  for the Murchison gold data against distance to the nearest fault, with short distances treated as favorable to gold. The curve was computed using the continuous spatial coordinates according to (22)–(23). A very similar result is obtained for the discretised presence-absence data. Effectively, the figure plots the proportion of known gold deposits within a certain distance from the nearest fault, against the corresponding fraction of survey area, for each threshold of distance to the nearest fault. For example, 10% of the survey area,  $p = 0.1$ , contains about 50% of known gold deposits,  $R(p) = 0.495$ . This curve contains much of the essential information required for geological prospectivity analysis [Baddeley, 2018]. The steep initial part of the curve indicates that proximity to the faults is highly prospective for deposits, in the sense that a large fraction of known deposits occur in a relatively small fraction of survey area situated within a relatively short distance from major faults. However the curve does not show the distance threshold value.

#### 4.2.3 Gastric mucosa data

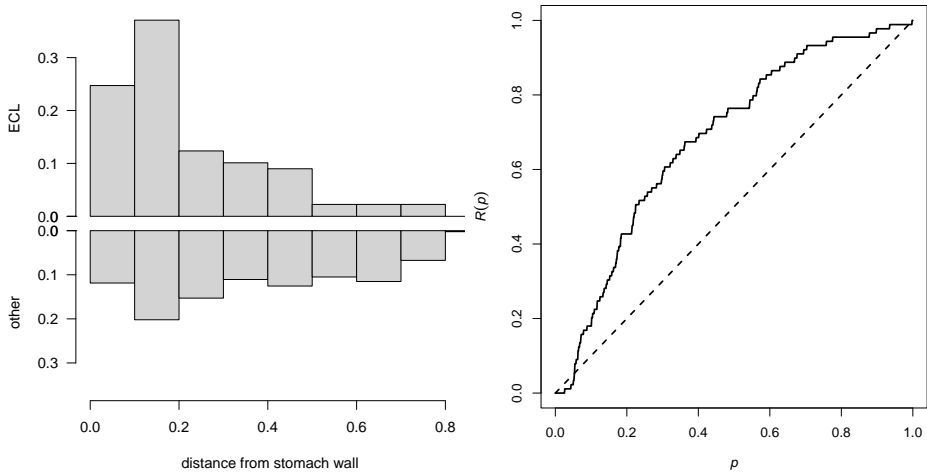


Figure 6: Analysis of gastric mucosa data of Figure 2 using the vertical coordinate  $y$  which represents distance from the stomach wall. *Left*: normalised histograms of  $y$  coordinates of ECL cells (upper histogram) and other cells (lower histogram). *Right*: C-ROC curve for  $y$  coordinate for ECL cells relative to other cells, treating lower values of  $y$  as favorable to ECL cells.

The right panel of Figure 6 shows the empirical C-ROC curve for the biological cells example of Figure 2. In this example  $y_j$  is the class of the  $j$ ’th cell ( $y_j = 1$  for ECL and  $y_j = 0$  otherwise),  $s_j$  is the vertical coordinate (distance to the stomach wall) treating short distances as favorable to ECL cells (so the inequalities in (4) and (5) are reversed). The C-ROC curve lies well above the diagonal which gives strong evidence that ECL cells have a greater preference for locations near the stomach wall than do the other cells. This is also apparent in the left panel of Figure 6 where the distribution of distances for is much more concentrated at small values for ECL cells than for other cells (more than 60% of ECL cells versus just over 30% of other cells are within distance 0.2 of stomach wall).

### 4.3 Variance

#### 4.3.1 Mapped point patterns and presence-absence data

For a mapped point pattern in a study region  $W$ , the false positive rate  $\text{FP}(t)$  is determined by the spatial cumulative distribution function of  $Z$  over  $W$ , and is not subject to random variability. If the point process  $X$  generating the

observed data is a Poisson process (or at least if, conditionally on the total number of points, the point locations are i.i.d.) then the conditional variance of  $\widehat{\text{TP}}(t)$  for fixed  $t$  given the total number of points  $n$  is the binomial variance

$$\text{var}[\widehat{\text{TP}}(t) \mid N = n] = \frac{1}{n} \text{TP}(t)(1 - \text{TP}(t)). \quad (25)$$

Consequently the C-ROC curve  $R_{Z,X}(p) = \widehat{\text{TP}}(\text{FP}^{-1}(p))$  has conditional variance

$$\sigma^2(p) = \text{var}[\widehat{R}(p) \mid N = n] = \frac{1}{n} R(p)(1 - R(p)). \quad (26)$$

For presence-absence data, if the indicators  $y_j$  for different pixels  $j$  are independent random variables, then the above expressions are expected to be the large-sample asymptotic variances, but a formal proof of this is outside of the scope of this manuscript.

In applications one can use the plug-in estimate  $\widehat{\sigma}^2(p) = n^{-1} \widehat{R}(p)(1 - \widehat{R}(p))$ .

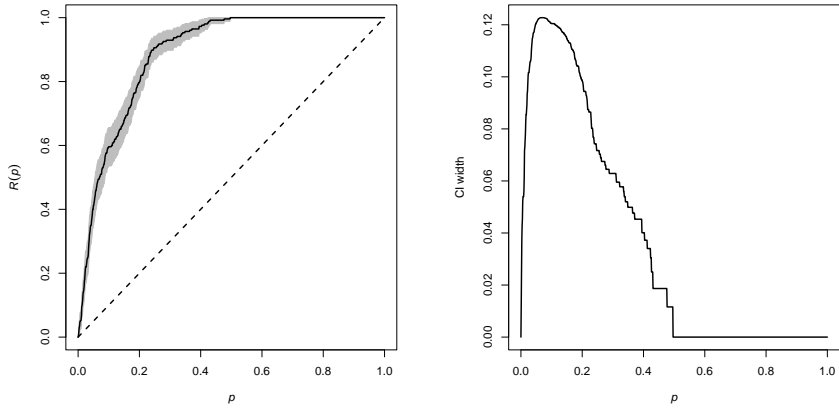


Figure 7: *Left:* C-ROC curve (calculated by raw method) for the Murchison gold data and the distance-to-nearest-fault covariate (solid lines) and pointwise approximate 95% confidence bands (grey shading) calculated using the plug-in estimate of (26). *Right:* width of confidence bands.

The left panel of Figure 7 shows pointwise approximate 95% confidence bands for the C-ROC curve for the Murchison gold data using the distance to nearest fault as the covariate. Note the optical illusion that the confidence intervals appear to be extremely narrow; this arises because the C-ROC curve has a steep slope. The right panel shows the actual width of the confidence bands as a function of  $p$ .

#### 4.3.2 Case-control data

If the cases and controls are mapped spatial point patterns, assume that they are generated by two independent Poisson point processes. Then the observed values of  $Z$  at the cases and the controls are i.i.d. samples of size  $n$  and  $m$  from distributions with unknown c.d.f.'s  $F$  and  $G$  respectively.

Then conditional on the sample sizes and following Hall et al. [2004] the large-sample asymptotic variance of the C-ROC curve is

$$\sigma^2(p) = \text{var}[\widehat{R}(p) \mid N = n, M = m] = n^{-1} R(p)(1 - R(p)) + m^{-1} \frac{f(G^{-1}(1 - p))^2}{g(G^{-1}(1 - p))^2} p(1 - p), \quad (27)$$

where  $f$  and  $g$ , respectively, are the densities corresponding to  $F$  and  $G$ .

Hall et al. [2004] proposed estimating  $f$  and  $g$  by kernel smoothing, and integrating these function estimates to obtain estimates of  $F$  and  $G$ . This yields a smooth estimate of the C-ROC curve, and also a plug-in estimate of the variance using (27), as detailed below.

Let  $\kappa$  be the template smoothing kernel, a probability density function on the real line, and let  $\mathcal{K}$  be the corresponding cumulative distribution function. Then the smoothed empirical estimators are

$$\tilde{F}(t) = \frac{1}{nh_1} \sum_{i=1}^n \mathcal{K}\left(\frac{t - Z(x_i)}{h_1}\right), \quad \tilde{G}(t) = \frac{1}{mh_2} \sum_{i=1}^m \mathcal{K}\left(\frac{t - Z(x_{n+i})}{h_2}\right), \quad (28)$$

where  $h_1$  and  $h_2$  are bandwidths. Methods for bandwidth selection are discussed by Altman and Leger [1995], Lloyd [1998]. The smooth estimate of the C-ROC curve is

$$\tilde{R}(p) = 1 - \tilde{F}_Z(\tilde{G}^{-1}(1 - p)). \quad (29)$$

To obtain the estimate of  $\sigma^2(p)$ , the squared gradient term  $f(G^{-1}(1 - p))^2/g(G^{-1}(1 - p))^2$  is computed using kernel estimates  $\tilde{f}$  and  $\tilde{g}$  with bandwidths  $h_f$  and  $h_g$  which may be different from the bandwidths  $h_1, h_2$  used above. The plug-in estimator of  $\sigma^2(p)$  using these smooth estimates is

$$\tilde{\sigma}^2(p) = n^{-1}\tilde{R}(p)(1 - \tilde{R}(p)) + m^{-1}\frac{\tilde{f}(\tilde{G}^{-1}(1 - p))^2}{\tilde{g}(\tilde{G}^{-1}(1 - p))^2}p(1 - p). \quad (30)$$

Asymptotic  $(1 - \alpha)$ -level confidence bands are given by  $\tilde{R}(p) \pm z_{\alpha/2}\tilde{\sigma}(p)$ , where  $z_\alpha$  is the upper  $1 - \alpha$  point of the standard normal distribution. The coverage of the confidence bands crucially depends on the bandwidths used in calculating  $\tilde{R}$  and  $\tilde{\sigma}^2$ . The optimal bandwidth for  $\tilde{R}(p)$  is described in Hall and Hyndman [2003], while Hall et al. [2004] make detailed recommendations on bandwidth selection for computing  $\tilde{\sigma}^2$ .

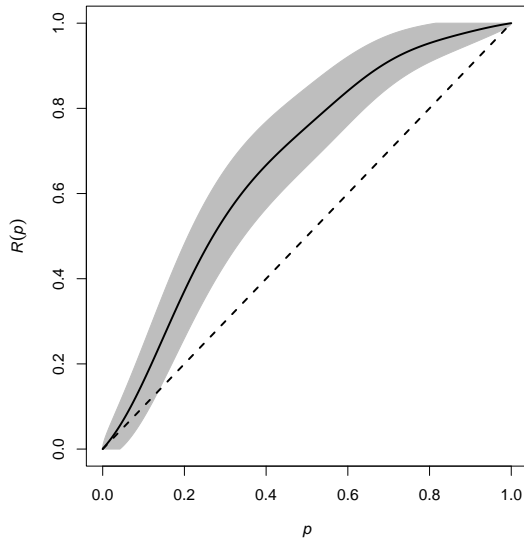


Figure 8: Kernel smoothing estimate (solid line) and pointwise 95% confidence bands (grey shading) calculated using (30), for the C-ROC curve for the mucosa case-control data against vertical coordinate.

Figure 8 shows a smoothed estimate of the C-ROC curve for the mucosa data (treating ECL cells as cases, and other cells as controls) using the  $y$  coordinate as the covariate. Grey shading shows pointwise 95% confidence bands for the true C-ROC curve based on the estimate of asymptotic variance (30) and truncated to  $[0, 1]$ . The bandwidths  $h_1, h_2$  were determined by Silverman's rule of thumb [Silverman, 1986, eq. (3.31), p. 48] applied separately to the  $y$ -coordinates of the ECL cells and the other cells, respectively.

## 4.4 Interpretation of C-ROC and C-AUC

This section discusses the interpretation of the ROC and AUC for spatial point pattern data based on a spatial covariate  $Z$ , as defined above. Similar comments apply to the cases of presence-absence and spatial case-control data.

### 4.4.1 Invariance under rescaling and transformation

**Lemma 1.** *Let  $Z$  be a spatial covariate on a domain  $W$ , and  $h : \mathbb{R} \rightarrow \mathbb{R}$  a strictly increasing transformation. Define the covariate  $Z^\dagger$  by  $Z^\dagger(u) = h(Z(u))$  for  $u \in W$ . Then the covariates  $Z$  and  $Z^\dagger$  have the same C-ROC curve, that is  $R_{Z,\mathbf{x}}(p) \equiv R_{Z^\dagger,\mathbf{x}}(p)$ .*

*Proof.* The ROC curve for  $Z^\dagger$  is a plot of  $\text{TP}^\dagger(t)$  against  $\text{FP}^\dagger(t)$  for all  $t \in \mathbb{R}$ , where from (22) and (23)

$$\text{TP}^\dagger(t) = \frac{1}{n} \sum_{i=1}^n \mathbf{1}\{Z^\dagger(x_i) > t\}, \quad \text{FP}^\dagger(t) = \frac{1}{|W|} \int_W \mathbf{1}\{Z^\dagger(u) > t\} du.$$

For any  $t \in \mathbb{R}$  and  $u \in W$  we have  $Z^\dagger(u) > t$  iff  $Z(u) > h^{-1}(t) = s$ , say, because  $h$  is 1–1. Hence  $\text{TP}^\dagger(t) = \text{TP}(s)$  and  $\text{FP}^\dagger(t) = \text{FP}(s)$ . Hence the ROC curves  $R_{Z,\mathbf{x}}(p)$  and  $R_{Z^\dagger,\mathbf{x}}(p)$  are identical.  $\square$

In particular Lemma 1 applies to numerical rescaling of the covariate:  $R_{Z,\mathbf{x}}(p) = R_{aZ+b,\mathbf{x}}(p)$  for any scale factor  $a > 0$  and any constant  $b$ .

**Lemma 2.** *The C-ROC is invariant under rescaling of the spatial coordinates, and under any area-preserving transformation of the spatial domain.*

*Proof.* More generally, let  $\psi : W \rightarrow W^*$  be a 1–1 transformation such that  $|\psi(B)| = c |B|$  for any measurable subset  $B \subseteq W$ , where  $c$  is a constant. Here  $\psi(B)$  denotes the image of  $B$  under the transformation,  $\psi(B) = \{\psi(x) : x \in B\}$ .

The data points  $x_i$  in  $W$  are transformed to data points  $y_i = \psi(x_i)$  in  $W^*$ , and the covariate  $Z$  on  $W$  is transformed to  $Z^*$  on  $W^*$  defined by

$$Z^*(v) = Z(\psi^{-1}(v)), \quad v \in W^*.$$

Consider the C-ROC curve based on

$$\text{TP}^*(t) = \frac{1}{n} \sum_{i=1}^n \mathbf{1}\{Z^*(y_i) > t\}, \quad \text{FP}^*(t) = \frac{1}{|W^*|} \int_{W^*} \mathbf{1}\{Z^*(v) > t\} dv.$$

We have  $Z^*(y_i) = Z(\psi^{-1}(y_i)) = Z(x_i)$  so that  $\text{TP}^* \equiv \text{TP}$ . Since  $\psi$  is area-preserving,  $\text{FP}^* \equiv \text{FP}$ . Hence the C-ROC curves are identical.  $\square$

Note that the C-ROC is *not* invariant under a geographic projection (change of spatial coordinates) unless it is area-preserving. In the discrete case, calculating the C-ROC using a grid of square pixels in latitude-longitude coordinate space would give greater weight to locations at higher latitudes; the calculation should be performed using a square grid in a conformal projection.

#### 4.4.2 Ranking ability

ROC and AUC are often claimed to be measures of “predictive power” [Lobo et al., 2007, Austin, 2007, Franklin, 2009]. However, it is clear that the ROC and AUC based on a covariate  $Z$  do not evaluate predictive ability in the conventional sense, because there is no predictive model in this context. A predictive model would give predictions of the presence probabilities at each pixel; a measure of predictive ability would indicate how well the observed pattern of presences and absences followed these predicted probabilities.

Rather, the C-ROC and C-AUC based on a covariate  $Z$  are measures of the “ranking ability” of  $Z$ , which is the extent to which presence and absence pixels in the study region would be segregated from each other, if pixels were sorted by increasing order of  $Z$ . Each point on the ROC curve represents a subdivision of the study region into two subregions of low and high values of  $Z$ , and measures the extent to which this subdivision separates space into regions of low and high density of points.

Since C-ROC and C-AUC are invariant under monotone transformations of the covariate, we could say that C-ROC and C-AUC measure the “ranking power” of **any** model  $\pi_j = \rho(z_j)$  where  $\rho(z)$  is a monotone increasing function of  $z$ . When there is such an underlying model the ROC curve in the right panel of Figure 5 is also known as the capture-efficiency curve as mentioned in Section 5.1.1.

In practice, the highest density of points could occur at locations where the covariate  $Z$  takes an intermediate value rather than a low or high value. For example, trees may be most abundant in locations which have moderate amounts of water, being neither arid nor swampy. The covariate would then have high value as a predictor in an appropriate model, but would not have high “ranking ability” as measured by C-ROC and C-AUC. In such a case a more appropriate approach would be to fit a model for the occurrence of points and then use the model ROC described in Section 5.

#### 4.4.3 Statistical interpretations

The C-ROC curve is nonparametric in nature; it does not assume any parametric form of dependence of the point pattern on the spatial covariate. The only implicit assumption is that larger values of the covariate are more favorable to the presence of points.

By construction, the C-ROC curve is insensitive to extremes, and to small sub-populations. In Appendix D we show an example, using the famous Chorley-Ribble cancer data, in which the ROC and AUC do not suggest any deviation from the diagonal line, but the effect of the covariate is statistically significant according to the likelihood ratio test. This can occur when the effect of the covariate only applies to a small fraction of the population.

As noted above, the C-ROC curve is a comparison of two distributions, namely, the distribution of the value of the covariate at a typical point of the pattern, and the distribution of the value of the covariate at a uniformly-randomly-selected point in the window.

**Lemma 3.** *For a spatial point pattern  $x = \{x_1, \dots, x_n\}$  in a study region  $W$ , and a spatial covariate  $Z(u)$  defined for all locations  $u \in W$ , let  $\widehat{TP}$  and  $\widehat{FP}$  be defined as in (22) and (23). Then*

1.  $F(t) = 1 - \widehat{TP}(t)$  is the cumulative distribution function of  $Z(x_I)$  where  $x_I$  is a uniformly-randomly-selected data point (i.e. where  $I$  is a uniformly random integer between 1 and  $n$ ).
2.  $G(t) = 1 - \widehat{FP}(t)$  is the cumulative distribution function of  $Z(U)$  where  $U$  is a uniformly-randomly-selected location in the window.
3. the C-ROC curve is a reversed P-P plot comparing the distribution of  $Z(x_I)$  to the distribution of  $Z(U)$ .

Similarly, given presence indicators  $y_j$  and covariate values  $z_j$  for  $j = 1, \dots, J$ , let  $\widetilde{TP}$  and  $\widetilde{FP}$  be defined as in (18) and (19). Then

4.  $F(t) = 1 - \widetilde{TP}(t)$  is the cumulative distribution function of the covariate value at a randomly selected 'presence' pixel, that is, the cdf of  $z_I$  where  $I$  is a random integer selected with uniform probability from the set  $\{j : y_j = 1\}$ ;
5.  $G(t) = 1 - \widetilde{FP}(t)$  is the cumulative distribution function of the covariate value at a randomly selected pixel, that is, the cdf of  $z_K$  where  $K$  is a random integer uniformly selected from 1 to  $J$ ;
6. the C-ROC curve is a reversed P-P plot comparing the distribution of  $z_I$  to the distribution of  $z_K$ .

*Proof.* Let  $I$  be a random integer between 1 and  $n$ , with equal probability for each possible outcome. Then the cumulative distribution function of  $Z(x_I)$  is

$$F(t) = \mathbb{P}\{Z(x_I) \leq t\} = \mathbb{E}\mathbf{1}\{Z(x_I) \leq t\} = \sum_{i=1}^n \mathbb{P}\{I = i\}\mathbf{1}\{Z(x_i) \leq t\} = \frac{1}{n} \sum_{i=1}^n \mathbf{1}\{Z(x_i) \leq t\},$$

and statement 1 follows. For statement 2, a uniformly random point  $U$  in  $W$  has probability density  $f(u) = \mathbf{1}\{u \in W\}/|W|$  in  $\mathbb{R}^2$  so that the cdf of  $Z(U)$  is

$$G(t) = \mathbb{P}\{Z(U) \leq t\} = \mathbb{E}\mathbf{1}\{Z(U) \leq t\} = \int_{\mathbb{R}^2} f(u)\mathbf{1}\{Z(u) \leq t\} du = \frac{1}{|W|} \int_W \mathbf{1}\{Z(u) \leq t\} du,$$

and statement 2 follows. Statement 3 is a trivial consequence. Statements 4–6 are proved in the same way.  $\square$

**Lemma 4.** *AUC can be interpreted according to (13) as the probability that a typical point of the point pattern has a higher value of the covariate than a uniformly-randomly-selected location in the window. That is,  $\text{AUC} = \mathbb{P}\{Z(x_I) > Z(U)\}$ , where  $x_I$  is a randomly-selected data point ( $I = 1, 2, \dots, n$  with equal probability) and  $U$  is a random point uniformly distributed in the window  $W$ .*

*Proof.* Let  $R(p)$  be the C-ROC curve, that is,  $R(p) = \text{TP}(\text{FP}^{-1}(p))$ . Then

$$\text{AUC} = \int_0^1 R(p) dp = \int_0^1 \text{TP}(\text{FP}^{-1}(p)) dp = \int_{-\infty}^{\infty} \text{TP}(t) d\text{FP}(t).$$

Invoking statements 1 and 2 of Lemma 3,

$$\text{AUC} = \int_0^1 \mathbb{P}\{Z(x_I) > t\} d\text{FP}(t) = \mathbb{P}\{Z(x_I) > Z(U)\},$$

where  $I$  and  $U$  are as described in Lemma 3.  $\square$

The C-ROC curve can also be expressed in terms of the Probability Integral Transformation.

**Lemma 5.** *The reverse C-ROC curve is the empirical cumulative distribution function of the values  $v_i = \text{FP}(z_i)$ , where  $z_i = Z(x_i)$  for  $i = 1, \dots, n$ .*

For the proof we notice that

$$R(p) = \text{TP}(\text{FP}^{-1}(p)) = \frac{1}{n} \sum_{i=1}^n \mathbf{1}\{Z(x_i) > \text{FP}^{-1}(p)\} = \frac{1}{n} \sum_{i=1}^n \mathbf{1}\{\text{FP}(Z(x_i)) > p\} = \frac{1}{n} \sum_{i=1}^n \mathbf{1}\{v_i > p\}.$$

Similarly  $R^<(p) = \frac{1}{n} \sum_{i=1}^n \mathbf{1}\{v_i \leq p\}$ .

## 4.5 Weaknesses

### 4.5.1 Dependence on study region

The ROC based on a covariate has the very important weakness that it depends on the choice of study region. (Similar warnings have been issued in the literature [Jiménez-Valverde, 2012] about the model ROC discussed in Section 5 below.)

The horizontal axis of the C-ROC plot is the fraction of area *in the study region* where the covariate exceeds a particular threshold. For example in the *Beilschmiedia* data the horizontal axis is the fraction of area of this particular rectangle, with its particular topography, where the terrain elevation or terrain slope exceeds a particular threshold. In the Murchison data, the horizontal axis is the fraction of area of the mapped rectangle, not the exploration lease, nor the prospective province.

This crucial fact is mainly attributable to inhomogeneity. The C-ROC expresses the ability of the covariate to segregate *the study region* into subregions of relatively high and low intensity of points. This ranking ability can only be high if there is substantial spatial variation in the intensity of points within the study region (the point process is “inhomogeneous”), and if there is spatial variation in the covariate values within the study region, and furthermore if high covariate values are associated with high intensity of points within the study region (or high covariate values are associated with low intensity of points).

To put it another way, the only case in which the C-ROC for a subregion is guaranteed to be the same as the C-ROC for the entire study region, is the case where the covariate has no effect and the C-ROC curve is the diagonal.

The C-ROC is completely bound to the choice of study region. Unlike a species distribution model, point process model or other statistical model, the C-ROC does not represent a scientific “law” that can be extrapolated from one study region to another, or considered to have validity independent of the choice of study region. Findings based on ROC/AUC cannot be generalised/extended to other contexts; they are completely bound to the original study region. In the *Beilschmiedia* data, the C-ROC for the terrain slope covariate does not express the intrinsic affinity or preference of individual trees for steep terrain. In spatial ecology we cannot use ROC analysis to predict the response of a species to climate change or habitat loss (or in general, any cases where the covariate values change over time) *even within the same spatial region*. In the Murchison data, the C-ROC for distance to nearest fault does not reveal a set of physical conditions which are always favorable to the presence of gold deposits. In exploration geology we cannot use ROC analysis to identify the best predictor variables for gold, except in the context of the original survey region (and not any subregion).

The fact that the C-ROC is bound to a particular study region only becomes an advantage when the objective is to segregate this specific region, for example, when it is desired to identify the most promising locations for mine exploration within an area that is available for mining, or when it is desired to find a location for a wind turbine which will minimise harm to wild bird life.

### 4.5.2 Restriction to a more homogeneous subset

In many real examples, the AUC decreases when we restrict attention to a sub-region of the original study region. This typically occurs when the density of points is more homogeneous in the sub-region.

In the Murchison data, the original study region is the bounding rectangle of the map data. For the distance-to-nearest-fault covariate, we obtain  $AUC = 0.89$  in this rectangle. The maximum covariate value (distance to nearest fault) in this rectangle is 128.9 km, while the maximum covariate value at a gold deposit point is 17.9 km. If we restrict attention to the region lying at most 20 km from the nearest fault, the AUC value falls to 0.79. This value drops further if we consider regions closer to the faults (0.71 for 10 km, 0.66 for 5 km). Figure 9 shows the C-ROC curves obtained by restricting attention to progressively shorter distances from the faults.

A synthetic example of the same phenomenon is shown in Appendix E.

### 4.5.3 Simpson’s Paradox

Since the C-ROC and C-AUC are completely bound to the choice of study region, we can expect paradoxes to arise when the study region is subdivided. These can be seen as instances of Simpson’s Paradox [Simpson, 1951, Yule, 1903].

Figure 10 shows a synthetic example. The unit square is divided into two subregions separated by the dashed lines. The intensity of points is uniform in each subregion, but different between the two subregions. In Figure 11 the left panel shows the C-ROC curve for the  $x$  coordinate, calculated for the entire dataset, with an AUC value of 0.73, indicating that the  $x$  coordinate has some predictive ability to separate the data into high- and low-intensity regions. However the middle and right panels show the C-ROC curves for the  $x$  coordinate calculated in the two subregions, indicating that within these subregions the  $x$  coordinate has no predictive value at all (AUC values 0.47 and 0.50).

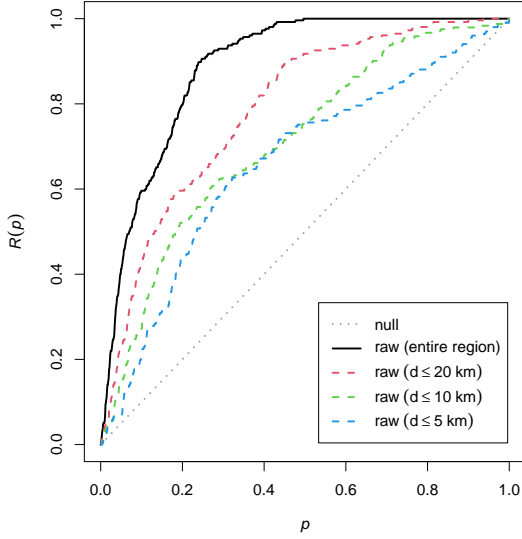


Figure 9: Effect of restriction to a subregion. C-ROC curves for the distance-to-nearest fault covariate in the Murchison data, computed for the entire study region (solid lines) and for regions where the distance to nearest fault is at most 20, 10 or 5 km (dashed lines). Corresponding AUC values are 0.89, 0.79, 0.71 and 0.66.

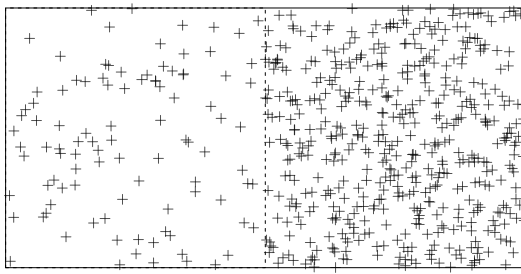


Figure 10: Synthetic example illustrating Simpson's Paradox for ROC.

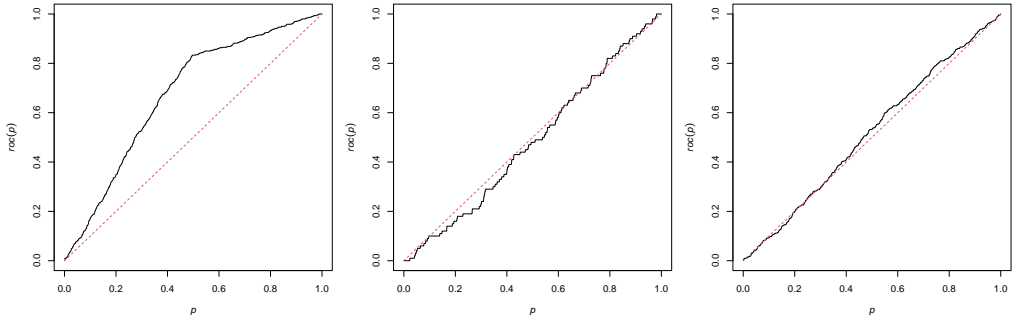


Figure 11: Demonstration of Simpson's Paradox for the data in Figure 10. ROC curves for the  $x$  coordinate calculated for the entire dataset (Left), for the left half (Middle) and the right half (Right). AUC values are respectively 0.67, 0.48, 0.51.

A describes the connection between the ROC curve for a full study region and the two ROC curves obtained when splitting the region into two disjoint subsets.

## 5 ROC for a fitted model

This section examines the particular version of the ROC curve that is most commonly used in species distribution modelling [Franklin, 2009, p. 222] and has been used in mineral prospectivity analysis [Porwal et al., 2010, Fabbri and Chung, 2008]. A predictive model (typically involving several explanatory variables) is fitted to a presence-absence dataset; the discriminant variable  $S$  is taken to be the *fitted presence probability* using the model, and the ROC curve compares the distributions of  $S$  at the “presence” and “absence” pixels. We call this the “model ROC” (M-ROC).

### 5.1 Definition

#### 5.1.1 Presence-absence pixel data

For presence-absence data (Section 3.2) we assume that a predictive model has been fitted. This may be a logistic regression, another binary regression, or any model which specifies the probability of presence  $\pi_j$  at each pixel  $Q_j$ . Let  $\hat{\pi}_j$  denote the predicted presence probability at  $Q_j$  according to the fitted model. The “model ROC curve” (M-ROC) is conventionally constructed from the estimates

$$\widehat{\text{TP}}(t) = \frac{\sum_{j=1}^J y_j \mathbf{1}\{\hat{\pi}_j > t\}}{\sum_{j=1}^J y_j}, \quad \widehat{\text{FP}}(t) = \frac{\sum_{j=1}^J (1 - y_j) \mathbf{1}\{\hat{\pi}_j > t\}}{\sum_{j=1}^J (1 - y_j)}. \quad (31)$$

Thus  $\widehat{\text{TP}}(t)$  is the fraction, of those pixels containing data points, in which the predicted probability of a data point exceeds  $t$ , and  $\widehat{\text{FP}}(t)$  is the fraction, amongst those pixels that do not contain data points, in which the predicted probability of a data point exceeds  $t$ . The M-ROC curve is the reverse P-P plot comparing the distributions of the *fitted presence probability*  $\hat{\pi}_j$  over pixels that do and do not contain data points. If pixels are sorted into increasing order of  $\hat{\pi}_j$ , then M-ROC and M-AUC measure how well this ordering segregates “presence” from “absence” pixels. In our shorthand, this empirical M-ROC curve based on a fitted model with presence probability vector  $\hat{\pi}$  will be denoted  $R_{\hat{\pi}, y}(p)$ .

Geologists use the terms “fitting rate curve” [Fabbri and Chung, 2008], “prediction rate curve” [Carranza, 2009b], “capture efficiency curve” [Porwal et al., 2010] and “frequency-area curve” [Ford et al., 2019] for a plot of the fraction of pixels containing deposits against the fraction of area captured by thresholding the fitted probability according to a model. The area fraction is computed using both “deposit” (presence) and “barren” (absence) pixels; that is,  $\widehat{\text{FP}}(t)$  in (31) is replaced by  $\widetilde{\text{FP}}(t)$  in (19) with  $z_j$  defined as  $\hat{\pi}_j$ . Nykänen et al. [2015] identify this as a version of the ROC curve, and point out the practical advantage of using  $\widetilde{\text{FP}}(t)$ , which can be based on a random sample of locations, instead of  $\widehat{\text{FP}}(t)$ , which requires finding “true negative” pixels.

If the true probabilities  $\pi$  were known, one could define the “true” or “theoretical” M-ROC curve  $R_{\pi, \pi}(p)$  constructed from

$$\text{TP}(t) = \frac{\sum_{j=1}^J \pi_j \mathbf{1}\{\pi_j > t\}}{\sum_{j=1}^J \pi_j}, \quad \text{FP}(t) = \frac{\sum_{j=1}^J (1 - \pi_j) \mathbf{1}\{\pi_j > t\}}{\sum_{j=1}^J (1 - \pi_j)}. \quad (32)$$

Under suitable conditions,  $R_{\hat{\pi}, y}(p)$  is a consistent estimate of  $R_{\pi, \pi}(p)$  if the model is true.

One statistical consideration is the risk of overfitting, since the fitted presence probability  $\hat{\pi}_j$  could depend strongly on the observed response  $y_j$ , causing  $\widehat{\text{TP}}(t)$  to be inflated and  $\widehat{\text{FP}}(t)$  to be deflated, causing bias in the M-ROC curve. Overfitting could be a severe problem with nonparametric models, or parametric models with many degrees of freedom, or small datasets. A standard remedy is to use the *leave-one-out* fitted value  $\hat{\pi}_j^{-j}$  calculated by fitting the model to all of the data except the data from pixel  $j$ , then predicting the probability at pixel  $j$  using the covariates in pixel  $j$ . Thus  $\hat{\pi}_j$  in (31) would be replaced by  $\hat{\pi}_j^{-j}$ . In our experience with real data, using the leave-one-out procedure has a visible but modest effect on the ROC curve. The change in the AUC value is small, typically less than 0.01. The AUC may either increase or decrease. See Figure 13 for an example.

When a model has been fitted, another estimate of the true M-ROC curve is the “**model-predicted**” M-ROC curve, which is the theoretical M-ROC curve determined by the fitted model. This is based on

$$\text{TP}(t) = \frac{\sum_{j=1}^J \hat{\pi}_j \mathbf{1}\{\hat{\pi}_j > t\}}{\sum_{j=1}^J \hat{\pi}_j}, \quad \text{FP}(t) = \frac{\sum_{j=1}^J (1 - \hat{\pi}_j) \mathbf{1}\{\hat{\pi}_j > t\}}{\sum_{j=1}^J (1 - \hat{\pi}_j)} \quad (33)$$

which we shall denote  $R_{\hat{\pi}, \hat{\pi}}(p)$ . Under suitable conditions, the model-predicted M-ROC  $R_{\hat{\pi}, \hat{\pi}}(p)$  is a pointwise consistent estimator of the true M-ROC  $R_{\pi, \pi}(p)$  provided the model is true.

### 5.1.2 Continuous mapped point pattern data

For a mapped point pattern  $x$ , instead of a model predicting the probability of presence in each pixel, we will have a model specifying the point process intensity  $\lambda(u)$  at each spatial location  $u$ . The empirical M-ROC will be formed from

$$\widehat{\text{TP}}(t) = \frac{1}{n} \sum_{i=1}^n \mathbf{1}\{\widehat{\lambda}^{-i}(x_i) > t\}, \quad \widehat{\text{FP}}(t) = \frac{1}{|W|} \int_W \mathbf{1}\{\widehat{\lambda}(u) > t\} du \quad (34)$$

where  $\widehat{\lambda}^{-i}(x_i)$  denotes the leave-one-out estimate of intensity at location  $x_i$  based on the point pattern data excluding  $x_i$ . Here  $\widehat{\text{TP}}(t)$  is the fraction of data points at which the fitted intensity value exceeds the threshold, and  $\widehat{\text{FP}}(t)$  is the fraction of area in the study region where the fitted intensity function value exceeds the threshold. In our shorthand, the empirical M-ROC curve based on a fitted model with intensity  $\widehat{\lambda}$  fitted to a point pattern  $x$  will be denoted  $R_{\widehat{\lambda},x}(p)$ .

The theoretical M-ROC will be formed from

$$\text{TP}(t) = \frac{\int_W \mathbf{1}\{\lambda(u) > t\} \lambda(u) du}{\int_W \lambda(u) du}, \quad \text{FP}(t) = \frac{1}{|W|} \int_W \mathbf{1}\{\lambda(u) > t\} du \quad (35)$$

and will be denoted  $R_{\lambda,\lambda}(p)$ . When a model has been fitted, the model-predicted M-ROC, denoted  $R_{\widehat{\lambda},\widehat{\lambda}}(p)$ , is formed similarly, with  $\lambda$  replaced by  $\widehat{\lambda}$  in (35).

### 5.1.3 Case-control point pattern data

For spatial case-control point pattern data, analysed conditionally on the spatial locations as described in Section 3.5.4, a model specifies the probability  $\pi_j = \mathbb{P}\{m_j = 1\}$  that location  $x_j$  is a case, for  $j = 1, \dots, J$ . The theoretical and empirical M-ROC curves are then constructed using the same formulas as for pixel data in Section 5.1.1: (32) and (31), with  $y_j = m_j = 1$  indicating that a point (rather than a pixel) is a case rather than a control ( $y_j = m_j = 0$ ). The interpretation of the rates, M-ROC and M-AUC is analogous to the pixel case with case and control locations taking the role of presence and absence pixels, respectively. Overfitting may occur in this context and we again recommend the use of leave-one-out estimates  $\widehat{\pi}_j^{-j}$ .

## 5.2 Examples

Consider the logistic regression model (14) for presence of *Beilschmiedia* in 10-metre pixels as a function of terrain elevation. The left panel of Figure 12 shows the M-ROC curve for this model, constructed according to standard practice in statistical ecology [Franklin, 2009, p. 222]; this is an ROC curve comparing the values of the fitted probability of presence computed at the pixels where trees are present, against those values computed at the pixels where trees are absent. That is, the score  $s_j$  at pixel  $j$  is defined to be the fitted presence probability  $\widehat{\pi}_j$ ; the observed true positive rate  $\widehat{\text{TP}}(t)$  and false positive rate  $\widehat{\text{FP}}(t)$  are computed as in (31) and  $\widehat{\text{TP}}(t)$  is plotted against  $\widehat{\text{FP}}(t)$ . Leave-one-out estimates  $\widehat{\pi}_j^{-j}$  of the presence probabilities could have been used instead, as we recommend, but the discrepancy is negligible. The middle panel shows the same calculations for the logistic regression as a function of terrain slope.

Note that the left and middle panels of Figure 12 are identical to the left and middle panels of Figure 5, as a consequence of Lemma 7 in Section 5.4.2. On the other hand, the right-hand panel of Figure 12 is obtained when the model is multiple logistic regression with additive terms for terrain elevation and terrain slope, and this does not reduce to a C-ROC.

Interestingly, the right panel shows that the model with additive terms for elevation and slope has slightly less ranking ability than the model depending only on terrain slope. The coefficients of elevation and slope are positive in each fitted model, but larger slopes tend to occur at smaller elevations (correlation -0.36), so a model which is expected to produce a better fit actually exhibits worse ranking ability. For reference, the fitted presence probabilities for the three logistic regression models are shown in Appendix B.

For the exact spatial locations of the *B. pendula* trees, we may fit the corresponding loglinear Poisson point process models (16) and compute the M-ROC curves using (34). The resulting curves are very similar to those in Figure 12 which is expected since these models are the continuous analogues of the models appearing in Figure 12.

For the model which is multiple logistic regression with additive terms for terrain elevation and terrain slope, Figure 13 shows the M-ROC curves computed using the raw estimator applied to the fitted probability of presence with and without the option of using a leave-one-out estimate. Somewhat surprisingly, the leave-one-out estimator produces a slightly more optimistic M-ROC curve with slightly higher AUC value, but as previously noted our

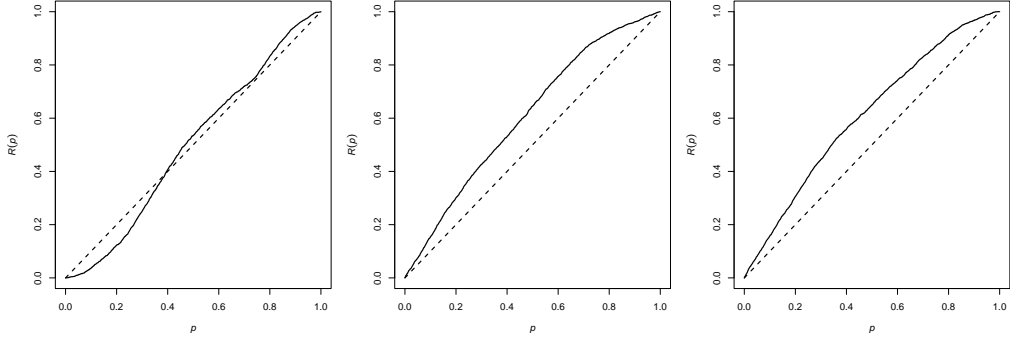


Figure 12: M-ROC curves for the logistic regression model of *Beilschmiedia* presence against terrain elevation (*Left*), against terrain slope (*Middle*), and against both terrain elevation and terrain slope (*Right*). Pixel size 10 metres. AUC values are 0.51, 0.61 and 0.61 respectively, Youden statistic values are 0.07, 0.20, 0.17 respectively. Note the left and middle panels are identical to the left and middle panels of Figure 5.

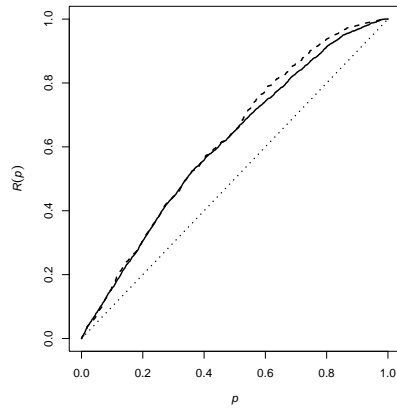


Figure 13: M-ROC curves for the logistic regression model of *Beilschmiedia* presence against both terrain elevation and terrain slope, using the conventional estimate (solid lines) and the leave-one-out estimate (dashed lines). Pixel size 10 metres.

experience with real data is that the leave-one-out estimator has a modest effect on the ROC curve and it may change AUC in either direction.

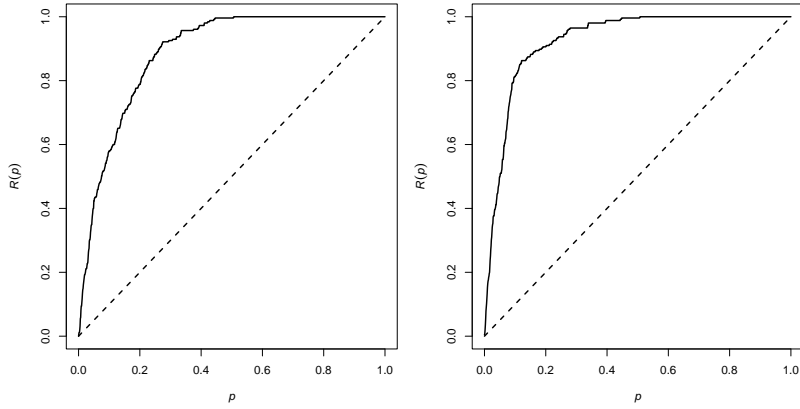


Figure 14: M-ROC curves for Poisson point process models for the Murchison gold deposits in which the intensity is a loglinear function of the distance to nearest fault (*Left*) or a log linear function of distance to nearest fault and greenstone indicator (*Right*). AUC values are 0.886 and 0.926 respectively. Youden statistic values are 0.647 and 0.742 respectively. Values at  $p = 0.1$  are 0.580 and 0.813 respectively. Note the left panel is identical to the right panel of Figure 5.

Figure 14 shows the M-ROC curves for the loglinear Poisson point process model for Murchison gold deposits as a function of distance to nearest fault  $D(u)$ , (left panel) and as a function of both distance to nearest fault and greenstone indicator (right panel). The right panel suggests substantially better performance for the small values of area fraction  $p$  which are of interest for geological exploration. For example at  $p = 0.1$  the curves in the left and right panels have height 0.580 and 0.813 respectively.

### 5.3 Variance

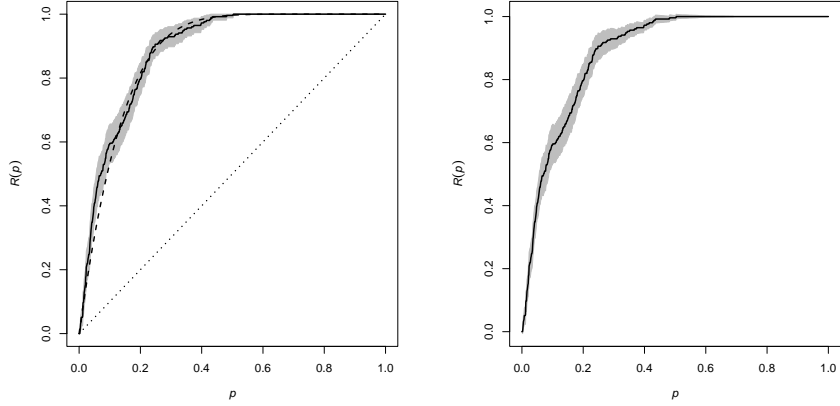


Figure 15: *Left:* M-ROC curve for the Poisson point process model fitted to the Murchison gold data assuming intensity is a loglinear function of distance-to-nearest-fault. Solid lines: M-ROC curve, raw estimate (leave-one-out). Grey shading: pointwise 95% confidence bands calculated using the plug-in estimate of asymptotic variance (26). Dashed lines: M-ROC curve predicted by model. *Right:* pointwise 95% confidence bands based on Monte Carlo variance estimate.

The left panel of Figure 15 shows ROC curves for the Poisson point process model fitted to the Murchison gold data assuming intensity is a loglinear function of distance-to-nearest-fault. Solid lines show the raw estimate (34) of the M-ROC curve for the fitted model, calculated using leave-one-out estimates of intensity. Dashed lines show the predicted M-ROC curve  $R_{\hat{\lambda}, \hat{\lambda}}(p)$  of the fitted model, which is based on (35) with  $\lambda$  replaced by  $\hat{\lambda}$ . Grey shading shows asymptotic pointwise 95% confidence bands around the raw estimate, calculated for the Poisson model using the plug-in estimate of asymptotic variance (26), ignoring variability due to parameter estimation. The right panel of Figure 15 shows pointwise 95% confidence bands around the raw estimate based on Monte Carlo estimates of pointwise variance, based on simulations of the fitted Poisson process model, suggesting that the asymptotic variance approximation is acceptable. The Monte Carlo approach has the advantage that it can easily be applied to other point process models and that it takes the extra variability due to parameter estimation into account.

The extra source of variability associated with the model fit is hard to analyse in any generality because it depends on the kind of model and the method of fitting the model. In large samples, this source of variability is expected to be negligible relative to the variances given in (25) and (26) so that the same expressions can be used. If there is only one covariate, and the model intensity is always a monotone increasing function of the covariate, then this source of variability collapses, because the M-ROC is identical to the C-ROC, see Section 5.4.2, and the variance of the M-ROC is identical to the variance of the C-ROC.

### 5.4 Interpretation of ROC for a fitted model

The central question is whether these curves can be used for model criticism or model selection, and in what way.

#### 5.4.1 M-ROC is insensitive to the model

**Lemma 6.** *The M-ROC for a model with fitted presence probabilities  $\hat{\pi}_j$  is identical to the M-ROC for another model with fitted presence probabilities  $\hat{\pi}_j^*$ , if  $\hat{\pi}_j^*$  is a strictly increasing function of  $\hat{\pi}_j$ , that is  $\hat{\pi}_j^* = \Psi(\hat{\pi}_j)$  where  $\Psi(p)$  is a strictly increasing function of  $p$ .*

*Proof.* For any threshold  $t \in \mathbb{R}$  we have

$$\hat{\pi}_j > t \quad \text{iff} \quad \hat{\pi}_j^* > \Psi^{-1}(t) = s$$

so that the M-ROC curves are identical.  $\square$

Thus in Figure 12 each panel would be unchanged if the fitted presence probabilities were reduced by a factor of 10, or transformed by the square root, etc.

The M-ROC and M-AUC depend only on the normalised predictions  $\pi_j / \sum_k \pi_k$  or normalised intensity  $\lambda(u) / \int_W \lambda(v) dv$ , and cannot detect errors which introduce a multiplicative factor into the presence probability or intensity. Hence, the M-ROC is “not affected by species prevalence” [Manel et al., 2001]. Consequently an ROC analysis cannot be used to predict changes in species abundance.

This could be considered an advantage when dealing with sampling designs or modelling techniques which are only able to predict the presence probability up to an unknown constant factor. It is a disadvantage insofar as the M-ROC is insensitive to errors in quantitative prediction (such as over- or under-estimating species abundance) and cannot be used to compare the performance of two different models if the models are related by a monotone transformation.

The same M-ROC will often be obtained for different SDM techniques.

#### 5.4.2 Collapses to C-ROC

If there is only one explanatory variable  $Z$ , then the M-ROC curve is the *same for all models* which depend monotonically on  $Z$ . Such models cannot be distinguished from each other on the basis of the ROC curve or the AUC value.

For any such model, the M-ROC curve is the same as the C-ROC curve based on the covariate  $Z$ , and contains information only about the ranking ability of the covariate, not about the particular model.

**Lemma 7.** *Suppose there is only a single spatial covariate  $Z$ . Consider any model which depends only on  $Z$ , and only in a monotone fashion,  $\hat{\pi}_j = f(z_j)$  where  $f$  is a strictly increasing function. Then the empirical M-ROC  $R_{\hat{\pi},y}(p)$  defined by (31) is identical to the empirical C-ROC  $R_{Z,y}(p)$  defined by (4)–(5).*

*Proof.* For any threshold  $t \in \mathbb{R}$  we have

$$\hat{\pi}_j > t \quad \text{iff} \quad z_j > f^{-1}(t) = s$$

so that the ROC curves are identical.  $\square$

For example, for presence-absence data, if the model is logistic regression (14) and if  $\hat{\beta}_1 > 0$ , then the M-ROC collapses to the C-ROC. For continuous mapped point pattern data, if the model is a loglinear Poisson process (16) and if  $\hat{\beta}_1 > 0$ , then the M-ROC  $R_{\hat{\lambda},x}(p)$  defined by (34) is identical to the C-ROC  $R_{Z,x}(p)$  defined by (22)–(23).

Thus in Figure 12 the left and middle panels do not depend on the details of the fitted model, only on the explanatory variable.

#### 5.4.3 M-AUC does not measure goodness-of-fit

Fielding and Bell [1997] argue that AUC is a measure of *goodness-of-fit* of a predictive model. This is contested by Lobo et al. [2007, p. 146].

A straightforward way to see that the M-AUC cannot be a measure of goodness-of-fit for a fitted model is to consider the case where the model is true and the fitted model parameters are close to the true values. For presence-absence data, the M-ROC  $R_{\hat{\pi},y}(p)$  defined by (31) is close to the “true” or “theoretical” M-ROC  $R_{\pi,\pi}(p)$  defined by (32). Although the fitted model is almost perfectly correct, the associated M-AUC is not equal to 1, and could range anywhere between 1/2 and 1. The M-ROC and M-AUC simply reflect the spatial non-uniformity of the presence probabilities  $\pi_j$ . Similar comments apply for the case of spatial point pattern data.

#### 5.4.4 Dependent on study region

The M-ROC depends strongly on the choice of the study region: it is “region-specific” [Jiménez-Valverde, 2012]. The justification for this statement is the same as in Section 4.5.1.

Even if an SDM is perfectly correct, the AUC of this SDM will reflect how well the study region can be segregated. If we restrict attention to a more homogeneous sub-region, the AUC should be expected to decrease. See the synthetic example in Figure 30.

In general, if the study region is divided into sub-regions, the AUC values computed in the sub-regions will be different from each other, and different from the AUC computed for the entire study region, even if the fitted model is the same in each sub-region. Hence the AUC cannot be used to measure agreement between model and data, neither for testing purposes nor for cross-validation.

### 5.4.5 Ranking ability

It should now be clear that the interpretation of M-ROC and M-AUC as measuring “predictive ability” of a fitted model [Lobo et al., 2007, Austin, 2007, Franklin, 2009] is weak. Instead one should think of “ranking ability” as the qualitative ability to identify regions of relatively high or low density of points, rather than the ability to predict numerically the density of points. The following result connects the ROC to the Lorenz curve, a common measure of inequality, which reinforces the interpretation of the ROC curve as a measure of ranking.

**Lemma 8.** *For a point process model with intensity function  $\lambda(u)$ , the theoretical M-ROC  $R_{\lambda,\lambda}(p)$  is identical to the reverse Lorenz curve for the function  $\lambda(u)$ .*

*Proof.* Suppose  $w : W \rightarrow [0, \infty)$  is the spatially-varying density of “wealth”. Then the Lorenz curve [Lorenz, 1905] is the graph of  $F_1(t)$  against  $F_0(t)$  where

$$F_1(t) = \frac{\int_W w(u) \mathbf{1}\{w(u) \leq t\} du}{\int_W w(u) du}, \quad F_0(t) = \frac{1}{|W|} \int_W \mathbf{1}\{w(u) \leq t\} du.$$

For a spatial point process model with intensity  $\lambda(u)$ , the theoretical (model-predicted) M-ROC is the graph of  $\text{TP}(t)$  against  $\text{FP}(t)$  where  $\text{TP}(t)$  and  $\text{FP}(t)$  are given by (34). If we set  $w(u) = \lambda(u)$  for  $u \in W$ , the two curves are equivalent, apart from the reversal of the inequality from  $w(u) \leq t$  to  $\lambda(u) > t$ .  $\square$

In the discrete case of presence-absence data, a similar statement holds approximately, when all presence probabilities are sufficiently small.

### 5.4.6 M-ROC is more optimistic than C-ROC

It is a consequence of the Neyman-Pearson Lemma that the M-ROC is always more “optimistic” than the C-ROC for any spatial covariate in the same context [Krzanowski and Hand, 2009, pp. 24–25], [Egan, 1975, Pepe, 2003].

**Lemma 9.** *For a point process model with intensity function  $\lambda(u)$ , the theoretical M-ROC dominates the theoretical C-ROC for any spatial covariate  $Z(u)$ :*

$$R_{\lambda,\lambda}(p) \geq R_{Z,\lambda}(p) \quad \text{for all } 0 \leq p \leq 1. \quad (36)$$

*Consequently, the AUC associated with the M-ROC is always greater than or equal to the AUC associated with the C-ROC.*

*Proof.* For brevity, write  $I_A(f) = \int_A f(u) du$  for any subset  $A \subseteq W$  and any integrable function  $f$  on  $W$ , and  $L(f, t) = \{u \in W : f(u) > t\}$  for the upper level set. Let  $p \in [0, 1]$  be fixed. From (35) we have  $R_{\lambda,\lambda}(p) = I_{L(\lambda,t)}(\lambda)/I_W(\lambda)$  where  $t$  satisfies  $I_{L(\lambda,t)}(1)/I_W(1) = p$ . Similarly, from (24) and (23),  $R_{Z,\lambda}(p) = I_{L(Z,s)}(\lambda)/I_W(\lambda)$  where  $s$  satisfies  $I_{L(Z,s)}(1)/I_W(1) = p$ . The Neyman-Pearson Lemma states that, given two integrable functions  $f(u), g(u) \geq 0$  on  $W$ , considering all subsets  $A \subseteq W$  satisfying the constraint that  $I_A(g) = G$  where  $G$  is a fixed value, the subset that achieves the largest value of  $I_A(f)$  is of the form  $A = L(f/g, c)$  for some constant  $c$ . Applying the Neyman-Pearson Lemma to the case  $f(u) = \lambda(u)$  and  $g(u) \equiv 1$ , we find that  $A = L(\lambda, t)$  and  $B = L(Z, s)$  satisfy  $I_A(1) = I_B(1) = p|W|$  so that  $I_A(\lambda) \geq I_B(\lambda)$ , and therefore  $I_A(\lambda)/I_W(\lambda) \geq I_B(\lambda)/I_W(\lambda)$ , that is,  $R_{\lambda,\lambda}(p) \geq R_{Z,\lambda}(p)$ .  $\square$

## 6 Connection to hypothesis tests

To gain further insight about the ROC and AUC, we now study their connection to hypothesis tests.

### 6.1 AUC and the Wilcoxon-Mann-Whitney test

First we consider numerical data. For the ROC and AUC described in Section 2, we noted in Section 2.4 that the ROC is effectively a comparison between two probability distributions, namely the distributions of the statistic  $S$  in the Positive and Negative populations.

Hanley and McNeil [1982] show that AUC is proportional to the Wilcoxon rank sum test statistic (Mann-Whitney  $U$  statistic) of a difference between two groups. Assume that independent random samples are taken from the Positive and Negative groups, with sizes  $n_1$  and  $n_2$  respectively. The null hypothesis  $\mathcal{H}_0$  is that the distribution of the statistic  $S$  is the same in each group. The Wilcoxon-Mann-Whitney test statistic  $U_1$  is calculated by pooling the values of  $S$  obtained from the two groups, arranging these values into ascending order, and computing the sum of the ranks of the values from the Positive group. Large values of  $U_1$  favour the alternative hypothesis that values of  $S$  are higher in the Positive group than in the Negative group.

Hanley and McNeil [1982] show that  $\text{AUC} = U_1/(n_1 n_2)$ . Thus, AUC is a measure of departure from the null hypothesis of equality between two groups — what might be called a measure of *badness-of-fit* for the *null* model of equality. Larger values of AUC indicate greater discrepancy between the Positive and Negative groups, rather than indicating greater agreement with a particular alternative hypothesis.

Additionally Hand and Till [2001] note that the AUC is equivalent to the Gini index,  $G = 2\text{AUC} - 1$ , another index of discrepancy between two distributions.

These results may be applied to case-control data. Consider the mucosa data of Figure 2 consisting of two groups of cells labelled ECL and Other. Using the vertical coordinate  $y$  as the discriminant variable, the AUC is 0.726. The one-sided Wilcoxon rank sum test has  $p$ -value  $4.5 \times 10^{-9}$  indicating very strong evidence against the null hypothesis that the two types of cells have the same spatial distribution, in favour of the alternative that ECL cells tend to be relatively more abundant at higher values of  $y$ .

## 6.2 AUC and the Berman-Waller-Lawson test

Next we consider spatial point pattern data (Section 3.1). Berman [1986] developed two statistical tests for determining whether a mapped spatial point pattern depends on a spatial covariate. Independently Waller et al. [1992] and Lawson [1993] developed a similar test for presence-absence data, to determine whether the presence probability depends on a spatial covariate. The Lawson-Waller test is asymptotically equivalent to Berman's first test as pixel size tends to zero, so we shall focus on Berman's tests.

### 6.2.1 Derivation of Berman's tests

Suppose that a mapped point pattern  $\mathbf{x} = \{x_1, \dots, x_n\}$  has been observed in the study region  $W$ . The aim is to determine whether the intensity of points is homogeneous, or whether the intensity depends on the real-valued spatial covariate  $Z(u)$ .

The derivation of Berman's tests assumes that the point pattern is a realisation of a Poisson process  $\mathbf{X}$  in  $W$  with some (unknown) intensity function  $\lambda(u)$ ,  $u \in W$ . The null hypothesis is the assumption of "no effect", that is, the point process intensity is uniform:

$$\mathcal{H}_0 : \lambda(u) \equiv \lambda,$$

while the alternative hypothesis  $\mathcal{H}_1$  is that the intensity is not spatially constant, or more specifically that the intensity is a non-constant function of  $Z$ ,

$$\mathcal{H}_1' : \lambda(u) = \rho(Z(u)),$$

where  $\rho(z)$  is some unknown function that is not constant.

The total number of points in  $\mathbf{x}$  follows a Poisson distribution with mean  $\Lambda = \int_W \lambda(u) \, du$ , and given that there are exactly  $n$  points, their locations are i.i.d. with probability density  $\lambda(u)/\Lambda$ . Let  $z_i = Z(x_i)$  be the values of the covariate observed at the data points of  $\mathbf{x}$ . The key insight [Berman, 1986, Sec. 3.1] is that, under these assumptions, the values  $z_1, \dots, z_n$  are i.i.d. with cumulative distribution function

$$F(z) = \int_W \mathbf{1}\{Z(u) \leq z\} \lambda(u)/\Lambda \, du. \quad (37)$$

Under  $\mathcal{H}_0$  we have  $\lambda(u)/\Lambda \equiv 1/|W|$  and the distribution function  $F$  is

$$F_0(z) = \frac{1}{|W|} \int_W \mathbf{1}\{Z(u) \leq z\} \, du, \quad (38)$$

which can be interpreted as the distribution function of  $Z(U)$  where  $U$  is a randomly selected location, uniformly distributed in  $W$ . Under  $\mathcal{H}_1$  the values  $z_i$  have some other cumulative distribution function. Under  $\mathcal{H}_1'$  this distribution is a weighted distribution

$$F(z) = \frac{|W|}{\mu} \int_{-\infty}^z \rho(t) \, dF_0(t). \quad (39)$$

Under these assumptions, the values  $z_1, \dots, z_n$  are sufficient, so the test may be conducted using these values alone.

Therefore the problem reduces to testing whether the probability distribution of  $z_1, \dots, z_n$  conforms to the null distribution  $z_i \sim F_0$ . This can be performed using any of the classical tests of goodness-of-fit for real random variables [D'Agostino and Stephens, 1986, Read and Cressie, 1988].

Berman's first test (which he called the  $Z_1$  test) is based on a standardised version of the statistic  $S = \sum_i z_i$ . Under  $\mathcal{H}_0$  it follows from [Berman, 1986, p.57, eq 3.3], that  $S$  has mean and variance

$$\mathbb{E}[S] = \mu = \lambda \int_W Z(u) du \quad (40)$$

$$\text{var}[S] = \sigma^2 = \lambda \int_W Z(u)^2 du. \quad (41)$$

Estimating  $\hat{\lambda} = n/|W|$ , or conditioning on  $n$ , we may plug in to (40)–(41) and compute the standardised statistic  $T = (S - \mu)/\sigma$  whose null distribution is approximately standard normal.

In Berman's second test (which he called the  $Z_2$  test), the values  $z_i$  are first transformed to  $u_i = F_0(z_i)$ , the probability integral transformation for the null hypothesis. For simplicity we assume that  $F_0$  is continuous and strictly increasing. Under  $\mathcal{H}_0$ , the values  $u_1, \dots, u_n$  are i.i.d. and uniform on  $[0, 1]$ , with mean  $\mathbb{E}[U_i] = 1/2$  and variance  $\text{var}[U_i] = 1/12$ . Under  $\mathcal{H}_0$ , the sample mean  $\bar{U} = \frac{1}{n} \sum_i u_i$  has mean  $\mathbb{E}[\bar{U}] = 1/2$  and variance  $\text{var}[\bar{U}] = 1/(12n)$ . Accordingly the test statistic

$$V_2 = \sqrt{12n} \left( \bar{U} - \frac{1}{2} \right) \quad (42)$$

has null distribution approximately standard normal.

### 6.2.2 Connection to C-ROC

Connections between the C-ROC (Section 4) and Berman's tests are now clear.

**Lemma 10.** *Assume  $F_0$  is continuous and monotone increasing. Then*

1. *The empirical cumulative distribution function of the values  $u_1, \dots, u_n$  is*

$$\hat{G}(p) = \frac{1}{n} \sum_{i=1}^n \mathbf{1}\{u_i \leq p\} = \hat{F}(F_0^{-1}(p))$$

where  $\hat{F}(z)$  is the empirical cumulative distribution function of  $Z(x_1), \dots, Z(x_n)$ .

2.  $\hat{G}(p) = R_{Z,\mathbf{z}}^<(p)$ .

3. *The test statistic in Berman's second test is related to the AUC by*

$$V_2 = \sqrt{12n} \left( \frac{1}{2} - \text{AUC}^< \right) = \sqrt{12n} \left( \text{AUC}^> - \frac{1}{2} \right) \quad (43)$$

A sufficient condition for the continuity and monotonicity of  $F_0$  is that  $Z$  is Lipschitz continuous with nonzero gradient almost everywhere.

*Proof.* By the assumptions on  $F_0$  we have  $u_i \leq p$  if and only if  $F_0^{-1}(u_i) \leq F_0^{-1}(p)$  which is equivalent to  $z_i \leq F_0^{-1}(p)$  so that  $\hat{G}(p) = \hat{F}_1(F_0^{-1}(p))$ . The next statement follows. Using Fubini's Theorem it can be verified that  $\bar{u} = \int_0^1 (1 - \hat{G}(p)) dp$ . Consequently

$$V_2 = \sqrt{12n} \left( \bar{u} - \frac{1}{2} \right) = \sqrt{12n} \left( \frac{1}{2} - \int_0^1 R_{Z,\mathbf{z}}^<(p) dp \right) = \sqrt{12n} \left( \frac{1}{2} - \text{AUC}^< \right).$$

The last equation follows because  $\text{AUC}^< = 1 - \text{AUC}^>$ . □

For practical interpretation, the most important finding is that AUC is related to the test statistic for a goodness-of-fit test of the null hypothesis of uniform intensity, that is, the null hypothesis of "no effect" (no dependence on the covariate  $Z$ ), rather than a test of goodness-of-fit to a fitted model. The primary role of the covariate  $Z$  in Berman's tests is to define the *alternative* hypothesis, that is, the type of departure from the null hypothesis of uniformity against which the test is designed to be sensitive.

Berman's tests can also be viewed in the context of a parametric model as significance tests for an effect term in the model [Berman, 1986]. Assume that the intensity is a loglinear function of  $Z$  as in (16). Then the uniformly most

powerful test of  $\mathcal{H}_0^\dagger : \beta_1 = 0$  against  $\mathcal{H}_1^\dagger : \beta_1 < 0$  is Berman's first test. A similar statement holds for presence-absence data for the logistic regression model (14). As Berman notes, this test is not optimal against other kinds of departure from the null hypothesis. In an effort to improve performance against some alternatives, Berman proposes the second test based on  $V_2$ , and also recommends that the analyst should plot and inspect the empirical CDF  $\hat{G}(p)$  as a diagnostic.

Some practical examples follow. For the *Beilschmiedia* pattern in the left panel of Figure 1 using the terrain elevation covariate, Berman's first and second tests have two-sided  $p$ -values of 0.466 and 0.014 respectively. The discrepancy between these test outcomes arises because the loglinear model (16) is inappropriate; this is explained carefully by Berman [1986]. Using the terrain slope covariate, the corresponding  $p$ -values are effectively zero.

For the Murchison data using the distance-to-nearest-fault covariate, Berman's first and second tests have  $p$ -values effectively zero.

### 6.3 Insensitivity to dependence on other covariates

The C-ROC curve for a covariate  $Z$  represents the “effect” of  $Z$ , more precisely, the extent to which an increase in the value of  $Z$  is associated with increased probability of presence or increased point process intensity. The C-ROC is entirely insensitive to the possible effects of other covariates which may be present.

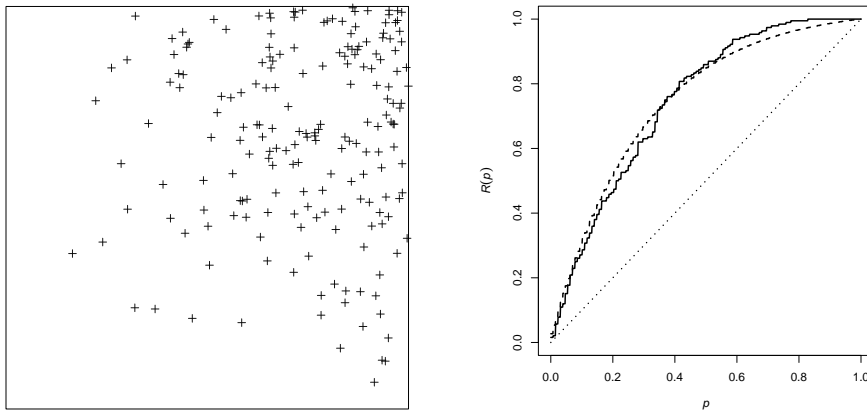


Figure 16: Insensitivity of C-ROC to other covariates. *Left:* Simulated point pattern with intensity depending on both the  $x$  and  $y$  coordinates. *Right:* empirical C-ROC curve based on the  $x$  coordinate.

Figure 16 shows a synthetic example. The left panel is a point pattern generated according to the intensity function  $\lambda(x, y) = 100x^2y$  in the unit square. The right panel shows the empirical M-ROC curve for the fitted loglinear Poisson model with intensity  $\lambda(x, y) = \exp(\beta_0 + \beta_1x)$  depending only on the  $x$  coordinate, which is also the empirical C-ROC curve based on the  $x$  coordinate. The corresponding AUC is 0.744. According to some writers, these results suggest a high level of “goodness of fit” of the fitted model. However, this is false for two reasons.

Firstly, as explained above, while the M-ROC curve does suggest that the point process intensity depends on  $x$ , it does not carry any information about the correctness or incorrectness of the functional form of the fitted model, because it collapses to the C-ROC curve based on the covariate  $x$ .

Secondly, the fact that the true intensity also depends on the  $y$  coordinate, is completely hidden in this analysis. A more appropriate test described in Baddeley et al. [2015, Sec. 10.3.5], using the  $y$  coordinate as the covariate for the test statistic, yields a  $p$ -value less than 0.0001, indicating strong evidence against the fitted model.

### 6.4 Youden index and Kolmogorov-Smirnov test

The Youden index was mentioned in Section 2.3 as an alternative to the AUC as a measure of ‘performance’. The Youden index is closely related to the Kolmogorov-Smirnov test [Kolmogorov, 1933, Smirnov, 1948]. In the general context of ROC and AUC for numerical data (Section 6.1), the Kolmogorov-Smirnov test of the null hypothesis that  $F \equiv F_0$  is based on the statistic  $\sqrt{n}D$ , where  $D$  is the maximum vertical separation between the graphs of  $\hat{F}(z)$  and  $F_0(z)$ :

$$D = \max_z |\hat{F}(z) - F_0(z)| = \max_p |\hat{F}(F_0^{-1}(p)) - p|. \quad (44)$$

The two-sided Youden index  $J$  is equivalent to  $D$  as defined above. The one-sided Youden index  $J_+$  defined in (7) is equivalent to the one-sided maximum deviation  $D_+ = \max_z(\hat{F}(z) - F_0(z))_+ = \max_p(\hat{F}(F_0^{-1}(p)) - p)_+$  and corresponds to the test statistic  $\sqrt{n}D_+$  for the one-sided Kolmogorov-Smirnov test [Baddeley et al., 2021].

Assuming that  $\hat{F}(z)$  is the empirical cumulative distribution function obtained from  $n$  independent realisations from  $F$ , the null distributions of  $\sqrt{n}D$  and  $\sqrt{n}D_+$  are known exactly. In the application to spatial point pattern data or spatial presence-absence data, this assumption is valid if the point process is Poisson, or the presence-absence indicators for different pixels are independent.

Thus the performance measures (AUC, Youden) for ROC curves are related to **tests of the presence of an effect** (Berman-Waller-Lawson, Kolmogorov-Smirnov), rather than measures of “goodness of fit” or a model. The AUC and Youden index are measures of the size of the effect, and are not adjusted for sample size.

For the *Beilschmiedia* pattern in the left panel of Figure 1 using the terrain elevation covariate, the Kolmogorov-Smirnov test has  $p$ -value less than 0.001. Likewise for the terrain slope covariate. Likewise for the Murchison data using the distance-to-nearest-fault covariate.

## 6.5 Other tests based on the spatial CDF

In addition to the Wilcoxon-Mann-Whitney and Kolmogorov-Smirnov tests, there are other hypothesis tests which have greater power against certain alternative hypotheses. These include the Cramér-Von Mises test [Cramér, 1928, von Mises, 1931] with test statistic

$$\omega^2 = n \int_{-\infty}^{\infty} [\hat{F}(z) - F_0(z)]^2 dF_0(z) = n \int_0^1 [\hat{F}(F_0^{-1}(p)) - p]^2 dp \quad (45)$$

and the Anderson-Darling test [Anderson and Darling, 1952, 1954] with test statistic

$$A = n \int_{-\infty}^{\infty} \frac{(\hat{F}(z) - F_0(z))^2}{F_0(z)(1 - F_0(z))} dF_0(z) = n \int_0^1 \frac{(\hat{F}(F_0^{-1}(p)) - p)^2}{p(1 - p)} dp. \quad (46)$$

Again the null distributions of these test statistics are known exactly, under the same assumptions as above.

For the *Beilschmiedia* data in the left panel of Figure 1 using the terrain elevation and terrain slope covariates, the Kolmogorov-Smirnov, Cramér-von Mises and Anderson-Darling tests all have  $p$ -values less than 0.001. Likewise for the Murchison data against distance to nearest fault.

## 6.6 M-ROC and M-AUC for a fitted spatial model

Fielding and Bell [1997] proposed that the AUC is a measure of goodness-of-fit for a species distribution model fitted to presence-absence data. In their context, this refers to the M-AUC, calculated using the fitted presence probabilities as the discriminant variable. The claim is that larger values of the M-AUC correspond to a better fit.

This is logically incompatible with the usual formulation of a goodness-of-fit test, in which the *null* hypothesis postulates that the data conform to the fitted model under consideration; the test statistic is a measure of *departure* from this null hypothesis; and large values of the test statistic indicate that the null hypothesis should be *rejected*. The model is deemed to be a good fit if the result of the goodness-of-fit test is *not* statistically significant.

Sections 6.2–6.5 above dealt with the C-AUC, but we argue below that the conclusions also apply broadly to the M-AUC. Then M-AUC is not a measure of goodness-of-fit of a fitted model of interest; rather it is a measure of departure from the null hypothesis of uniformity, and is related to a test of this null hypothesis.

A true test of goodness-of-fit, for a species distribution model or spatial point process model, would normally be based on a covariate *that is not used in the model*. In Section 6.2 we saw that the AUC is related to the Berman-Waller-Lawson test of the null hypothesis of *uniform* intensity (intensity not depending on any covariates) against the alternative that the intensity depends on a covariate  $Z$ . In that context, the covariate  $Z$  is extraneous to the null model whose goodness-of-fit is being tested.

Extending the results of Sections 6.2–6.5 to apply to the M-AUC is technically complicated, because the discriminant variable  $S = \hat{p}$  is data-dependent, so there is an additional source of variability associated with sampling error. Detailed analysis will depend on details of the model and the fitting algorithm.

This extra source of variability can be ignored entirely in the case where the model involves only one explanatory variable  $Z$ , and where the model states that the probability of presence is a monotonically increasing (or monotonically decreasing) function of  $Z$ . In that case, by Lemma 7, the M-ROC collapses to the C-ROC based on  $Z$ , and the results of Section 6.2 apply.

Similarly in a logistic regression or loglinear Poisson process model with multiple covariates, the M-ROC curve depends only on the direction  $\hat{\theta}/\|\hat{\theta}\|$  of the fitted coefficient vector  $\hat{\theta}$ , not on its magnitude  $\|\hat{\theta}\|$ . In other cases, the effect of sampling variability can be neglected to first order if we use the leave-one-out predictor  $\hat{\pi}_j^{-j}$ .

## 7 Connection to resource selection functions

This section explores the relationship between ROC curves and “resource selection functions”. The findings give guidance on how to interpret or “read” the ROC curve, and how to use the ROC curve for model checking.

### 7.1 Motivation

Inspection of the C-ROC or M-ROC curves is an indirect and impractical way of investigating the effect of covariates. Covariate values are not displayed in graphs of the ROC. For the C-ROC (Section 4) it would be possible to annotate the plot, adding the covariate values as tickmarks on the axes. However, for the M-ROC (Section 5), if the model involves more than one covariate, it becomes impractical to depict the mapping from covariate values to predicted values of presence probability.

The dependence of the presence/absence events on the spatial covariates is described by a species distribution model (SDM). In most SDM’s, the presence probability  $p$  at a given pixel is modelled as depending on the covariate values  $Z_1, \dots, Z_m$  at the same pixel, through a function

$$p = \rho(Z_1, Z_2, \dots, Z_m). \quad (47)$$

In various applications, the function  $\rho$  in (47) is called a *resource selection function* or *mineral potential map*.

For ecological applications, Manly [Manly et al., 1993, p. 177] defined a *resource selection function* (RSF) as “any function that is proportional to the probability of use by an organism”. Any function proportional to  $\rho$  in (47) could be called an RSF, and estimation of an RSF is equivalent to estimation of  $\rho$  up to a constant factor. The resource selection function value reflects preference for, or avoidance of, particular environmental conditions. Boyce et al. [2002, Sec. 1] say “RSF models can be powerful tools in natural resource management, with applications for cumulative effects assessment, land-management planning, and population viability analysis”. While RSF and SDM are closely related, the ecological literature seems to associate the terms RSF and SDM with *nonparametric* and *parametric* estimation, respectively.

In applications to mineral exploration, the function  $\rho$  in (47) is an index of the *prospectivity* [Bonham-Carter, 1995, Carranza, 2009a, Baddeley, 2018, Knox-Robinson and Groves, 1997] or *mineral potential* [Porwal et al., 2010, Ford et al., 2019], the predicted relative frequency of undiscovered deposits as a function of geological and geochemical covariates.

Similarly, the dependence of a spatial point pattern on spatial covariates is described by a point process model. In many such models, the intensity function of the model is a function of the covariates, in the form

$$\lambda(u) = \rho(Z_1(u), \dots, Z_m(u)), \quad u \in W \quad (48)$$

The function  $\rho$  in (47) or (48) can be estimated from data by parametric model-fitting or non-parametric estimation in various ways. Parametric modelling and model-fitting are discussed in Baddeley et al. [2015, Chap. 9]. Estimators of resource selection functions are discussed in Manly et al. [1993]. In the case of a single explanatory variable  $Z$ , nonparametric estimators of the function  $\rho$  were described by Baddeley et al. [2012], Baddeley [2018], Guan [2008], Guan and Wang [2010].

The left panel of Figure 17 shows three different estimates of the function  $\rho$  for the Murchison gold data using the distance to nearest fault as the covariate  $Z$ . We have used the point process formulation. That is, we assume the point process intensity  $\lambda(u)$  at a location  $u$  is related to the covariate  $Z(u)$  by  $\lambda(u) = \rho(Z(u))$ , where  $\rho$  is a function to be estimated. Thick solid lines show the kernel smoothing estimate of  $\rho$  proposed in Baddeley et al. [2012]. Dashed lines show the maximum likelihood estimate for the parametric model  $\rho(d) = \exp(\beta_0 + \beta_1 d)$  under the Poisson assumption corresponding to (16). Thin solid lines show a monotonic regression estimate proposed by Sager [1982] and adapted to this context by Baddeley [2018, Sec. 5]. The broad agreement between these estimates suggests that the parametric model would be adequate.

Related concepts include the “continuous Boyce index” proposed by Hirzel et al. [2006], which is an estimator of  $\rho(z)/\Lambda$ .

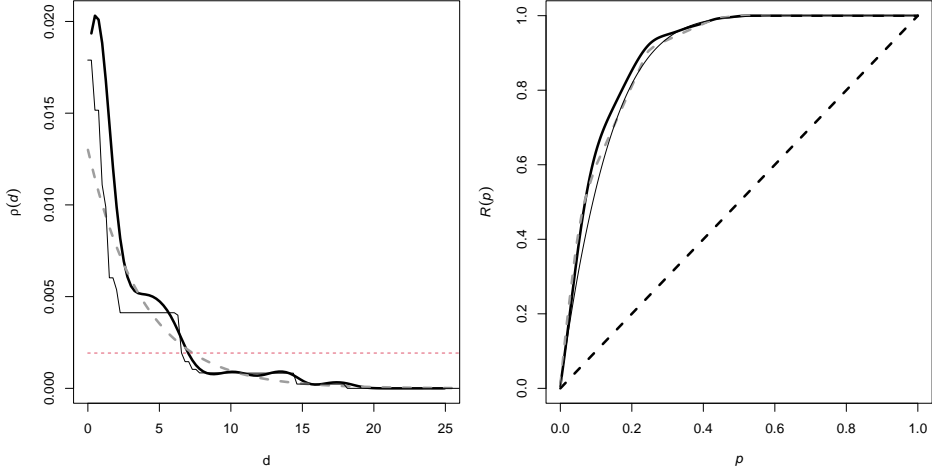


Figure 17: *Left:* Estimates of the function  $\rho(d)$  expressing the intensity of gold deposits as a function of distance to the nearest fault in the Murchison data. *Right:* corresponding C-ROC curves, computed from left panel using Proposition 1 equation (52). Thick solid lines: kernel smoothing estimate [Baddeley et al., 2012]. Thin solid lines: monotonic estimate [Sager, 1982, Baddeley, 2018]. Dashed lines: maximum likelihood estimate of loglinear function  $\rho(d) = \exp(\beta_0 + \beta_1 d)$  corresponding to logistic regression of presence-absence responses (Baddeley et al., 2015, Chap. 9, Baddeley et al., 2010).

## 7.2 Connection between $\rho$ and C-ROC

Here we establish a connection between  $\rho$  and the C-ROC curve. We shall focus on the continuous space (point process) case; the discrete case (presence-absence data) is similar.

For convenience we impose regularity assumptions. For a spatial covariate  $Z$ , we shall assume that  $\text{FP}(z)$  is differentiable. A sufficient condition is that  $Z : W \rightarrow \mathbb{R}$  be differentiable with nonzero gradient [Baddeley et al., 2012, Appendix A.1].

**Proposition 1.** *Let  $\lambda(u)$  denote the intensity function of a point process  $\mathbf{X}$ , and assume that the intensity is a function of a single spatial covariate  $Z$ , that is,*

$$\lambda(u) = \rho(Z(u)), \quad u \in W. \quad (49)$$

*Assume the regularity assumptions stated above. Then the theoretical C-ROC curve based on  $Z$  is differentiable, with slope*

$$\frac{d}{dp} R_{Z,\lambda}(p) = \frac{1}{\kappa} \rho(\text{FP}^{-1}(p)) \quad (50)$$

*where  $\kappa = \Lambda/|W|$  is the mean intensity of  $\mathbf{X}$ , and  $\text{FP}^{-1}$  is the left-continuous inverse function of  $\text{FP}(t)$  defined in (23). Here  $\Lambda$  is the expected number of points falling in  $W$ ,*

$$\Lambda = \int_W \lambda(u) \, du = \int_W \rho(Z(u)) \, du = \int_{-\infty}^{\infty} \rho(z) \, dF_Z(z) = - \int_{-\infty}^{\infty} \rho(z) \, d\text{FP}(z). \quad (51)$$

*The function in (50) is a probability density on  $[0, 1]$ . Conversely the theoretical C-ROC curve is determined by  $\rho$  through*

$$R_{Z,\lambda}(p) = \frac{1}{\kappa} \int_0^p \rho(\text{FP}^{-1}(v)) \, dv = - \frac{1}{\kappa} \int_{-\infty}^{\text{FP}^{-1}(p)} \rho(z) \, d\text{FP}(z). \quad (52)$$

*Proof.* For any realisation  $\mathbf{x}$  of the point process  $\mathbf{X}$  consider the corresponding values  $z_i = Z(x_i)$  of the covariate at the data points  $x_i \in \mathbf{x}$ . Then [Daley and Vere-Jones, 1988, p. 22] the values  $z_i$  constitute a point process on the real line, with intensity function  $h(z) = \rho(z)g_W(z)$  where  $g_W$  is the derivative of the unnormalised spatial cumulative distribution function of  $Z$  on  $W$ , that is,  $g_W = G'_W$  where  $G_W(z) = |W|(1 - \text{FP}(z))$ . Consequently

$$\text{TP}(z) = \frac{1}{\Lambda} \int_z^{\infty} h(z) \, dz = \frac{1}{\Lambda} \int_z^{\infty} \rho(z)g_W(z) \, dz$$

where

$$\Lambda = \int_W \lambda(u) du = \int_{-\infty}^{\infty} \rho(z) g_W(z) dz$$

so that  $\mathbf{TP}$  has derivative

$$\mathbf{TP}'(z) = \frac{d}{dz} \mathbf{TP}(z) = -\frac{1}{\Lambda} \rho(z) g_W(z) = \frac{|W|}{\Lambda} \rho(z) \mathbf{FP}'(z).$$

Using  $R_{Z,\lambda}(p) = \mathbf{TP}(\mathbf{FP}^{-1}(p))$ , the derivative of  $R_{Z,\lambda}(p)$  is

$$\frac{d}{dp} R_{Z,\lambda}(p) = \frac{\mathbf{TP}'(\mathbf{FP}^{-1}(p))}{\mathbf{FP}'(\mathbf{FP}^{-1}(p))} = \frac{\frac{|W|}{\Lambda} \rho(\mathbf{FP}^{-1}(p)) \mathbf{FP}'(\mathbf{FP}^{-1}(p))}{\mathbf{FP}'(\mathbf{FP}^{-1}(p))} = \frac{|W|}{\Lambda} \rho(\mathbf{FP}^{-1}(p)). \quad (53)$$

□

**Corollary 1.** *Under the assumptions of Proposition 1,*

1. *If the C-ROC curve is piecewise linear, then the  $\rho$  curve is piecewise constant.*
2. *If  $\rho$  is monotone increasing, the C-ROC curve is concave.*
3. *If  $\rho$  is monotone decreasing, the C-ROC curve is convex.*

*Proof.* The first statement is a direct application of (50), or see Baddeley et al. [2021]. The remaining statements are trivial applications of (52). □

**Lemma 11.** *Under the regularity assumptions stated above, the model-predicted M-ROC curve is always concave.*

*Proof.* Let  $\lambda(u)$  be the intensity function of the model, which may depend on any number of covariates  $Z_1, \dots, Z_m$ . Define the artificial covariate  $Y(u)$  to equal  $\lambda(u)$ . Then trivially  $\lambda(u) = \rho(Y(u))$  where  $\rho(y) = y$  is a strictly increasing real function. By Proposition 1 the model-predicted ROC curve of  $Y$  is concave. But the model-predicted ROC curve of  $Y$  is equivalent to the model-predicted model ROC curve. Hence the latter is concave. □

The results above were stated for the “true” or “expected” ROC curve and the corresponding “true” function  $\rho$ , and for the “true” or “predicted” ROC curve based on a model. The results may also be exploited when empirical estimates are available. For example, when empirical estimates of  $\rho$  are available, corresponding estimates of the ROC curve may be computed using equation (52). The right panel of Figure 17 shows the ROC curves computed, using equation (52), from the estimates of  $\rho$  in the left panel.

### 7.3 Interpretation of results

Proposition 1 provides further insight into properties of the ROC curve. By assumption,  $\rho(z)$  represents a general relationship that does not depend on the window, and describes how the point process depends on the covariate at every location. In contrast, the C-ROC curve is expressed in equation (52) in terms of  $\rho$ ,  $\kappa$  and  $\mathbf{FP}$ . By definition,  $\kappa$  and  $\mathbf{FP}$  depend on the choice of window  $W$ . This clarifies how the ROC curve depends on the choice of window, and explains why instances of Simpson’s Paradox can occur.

In principle,  $\rho$  could be estimated from data observed within one region, and the estimated relationship can be used to make predictions for another region. This implicitly assumes that the same relationship or “law” (48) holds within both regions, which may be plausible in some applications. Predictions made for a new region could include predictions of the ROC curve: for this we require only the spatial CDF of the covariate in the new region, and then we can apply Proposition 1.

Figure 18 shows estimates of  $\rho$  for the *Beilschmiedia* trees as a function of a single covariate, terrain elevation in the left panel and terrain slope in the right panel. The “rug plots” along the horizontal axes show the observed values of the covariate  $Z$  at the data points, and the grey shading shows the pointwise asymptotic 95% confidence interval described in Baddeley et al. [2012]. Refer to Figure 5 for the corresponding ROC curves.

The left panel of Figure 18 indicates that forest density is much higher at higher elevations, except for the very highest elevations. The right panel shows that forest density is very low on flat terrain, and that there is a slightly greater forest density on more sloping terrain. These observations could be influenced by the topography and hydrography of the current study area: the highest elevation in the study area is achieved on a plateau, and the lowest elevation appears to be a river, where trees of this type do not grow.

The left panel of Figure 18 suggests that forest density is not a monotone increasing function of terrain elevation. In the light of Corollary 1, this is confirmed retrospectively by the left panel of Figure 5.

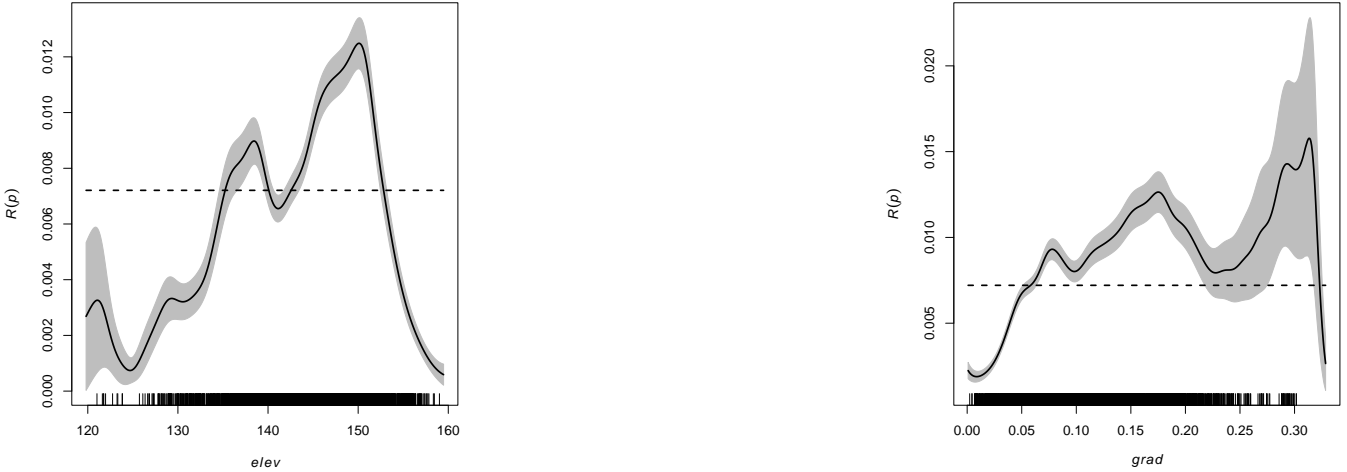


Figure 18: Estimates of the function  $\rho(d)$  expressing the intensity of *Beilschmiedia* trees as a function of terrain elevation (Left) or as a function of terrain slope (Right). Solid lines: kernel smoothing estimate [Baddeley et al., 2012]. Grey shading: pointwise 95% confidence interval.

These examples militate in favour of using estimates of  $\rho$ , rather than the ROC curve, for the initial exploration and modelling of dependence on covariates. The ROC is cumulative, and somewhat difficult to interpret, while  $\rho$  is proportional to the derivative of ROC, and is more straightforward. It is important to assess whether  $\rho(z)$  can be assumed to be a monotone function of  $z$ . The true merit of  $Z$  may be considerably greater than that suggested by AUC if  $\rho(z)$  is not monotone. If there is only a single covariate  $Z$ , then we should use ROC if there's good reason to believe that increasing values of  $Z$  are increasingly favorable. Otherwise, we should use  $\rho(z)$  to investigate. (Or compare empirical ROC with that based on monotone regression of  $\rho(z)$  (equivalent to convex regression of ROC): discrepancies suggest non-monotone  $\rho(z)$ .

An advantage of ROC over  $\rho$  is that ROC gives a sense of how much (area fraction) of the spatial domain is involved in each peak or trough of  $\rho$ .

## 8 Extensions of ROC curves

### 8.1 Restriction to a subset

As mentioned in Sections 4.5.1 and 5.4.4, both the C-ROC and M-ROC depend on the spatial domain over which they are calculated. This important fact can be turned to our advantage. Calculation of the ROC and AUC can be restricted to a subset  $B$  of the spatial domain  $W$ , simply by restricting the domains of summation and integration in any of the definitions (4)–(5), (22)–(23), (31), (34) or (35). Restriction to subsets can be useful in the same way that it is useful to break down an aggregate summary statistic into summaries for sub-populations.

Figure 19 shows the empirical ROC curves for subsets of the Murchison survey, namely the subsets inside and outside the greenstone outcrop. Within the greenstone outcrop, the distance to nearest fault is not very informative. However, outside the greenstone outcrop, the distance covariate is highly informative, and short distances are especially highly prospective for gold.

These findings are expected if we consider the three-dimensional geological structure near the surface. Our data are the two-dimensional projected locations of the gold deposits, and our covariates are the two-dimensional surface profiles of the solid greenstone and the fault planes. Assume that, in three dimensions, gold deposits are highly likely to lie inside greenstone, which in turn is highly likely to occur near a geological fault. Then in two dimensions, a location inside the greenstone outcrop is highly prospective for gold; a location outside the greenstone outcrop, but close to a geological fault, is more likely to lie above greenstone below the surface, so it is highly prospective for gold.

### 8.2 Weights on data points

For spatial point pattern data, numerical weights  $w_i \geq 0$  may be attached to the individual data points  $x_i, i = 1, \dots, n$ . The weights could represent multiplicity or severity (for example, number of people involved in each road accident),

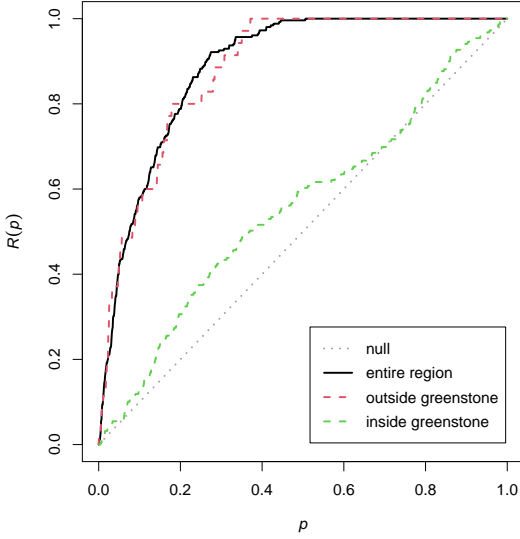


Figure 19: Empirical C-ROC curves  $R_{Z,x}^<(p)$  for subsets of the Murchison survey. *Black*: entire region; *red*: outside greenstone outcrop; *green*: inside greenstone outcrop. Covariate is distance to nearest fault, with small distances interpreted as more favorable to gold.

cost or value (the total amount of gold in each gold deposit, the estimated volume of each tree). They can also be used to adjust for uneven sampling effort or uneven probability of detection.

Weighted versions of the ROC curves can be defined by introducing numerical weights  $w_i$  into the calculation of the numerators of the true positive rates in each of the equations (22), (34) and (35). In the denominators,  $n = n(\mathbf{x})$  is replaced by  $\sum_i w_i$ . In equation (35), the intensity  $\lambda(u)$  of the point process  $\mathbf{X}$  is replaced by the intensity of the random measure assumed to have generated the points and weights (technical details are beyond the scope of this article).

For an intuitive appreciation of the weighted ROC, suppose that the data points are the home addresses of disease cases, and the weight at each address  $x_i$  is the number of cases at that address. Then the weighted ROC of a spatial variable  $Z$  for the weighted point pattern of home addresses is equivalent to the un-weighted ROC of  $Z$  for the individual cases. The weighted AUC is the probability that a randomly-selected *case* has a higher value of  $Z$  than a randomly-selected spatial location.

**Accounting for uneven sampling effort or detection probability** In some applications the probability of detecting a point is not constant but spatially varying. This may be a consequence of the detection technique, or may occur if the space was explored with uneven sampling effort. This contributes a bias to the observed “true positive rate”  $\widehat{TP}(t)$ .

The bias can be corrected using the Horvitz-Thompson device, that is, by weighting each observed point by the reciprocal of its detection probability,  $w_i = 1/q_i$  where  $q_i$  is the probability that a point at location  $x_i$  would have been detected. This probability must be known or calculable for all the observed points  $x_i$ , and must be nonzero for all spatial locations. This weight is applied to the calculation of  $\widehat{TP}(t)$  while the calculation of  $\widehat{FP}(t)$  is not changed.

For the ROC curve of a fitted model, the fitted model should also take the uneven sampling effort into account. In logistic regression or loglinear Poisson regression, the model should include an offset term equal to the logarithm of the sampling effort.

**Weighted presence-absence data** It is also possible to introduce weights for presence-absence data by multiplying the indicator function by an individual weight for each of the presence pixels in the calculation of the true positive rate. The weight may again indicate e.g. the number of cases in that pixel or the estimated volume of wood in that pixel.

### 8.3 ROC relative to a baseline

As previously mentioned for the C-ROC for point pattern data in Section 4.1.2 we have that  $1 - \text{FP}(t)$  is the c.d.f. of the covariate value  $Z(U)$  at a random location  $U$  uniformly distributed in  $W$ . However, in some contexts it may

be more natural to consider another reference distribution than the uniform. For example, consider the cases of a disease where the density of the susceptible population is proportional to a given baseline function  $b(u)$  for  $u \in W$ . Then we define  $R_{Z,x,b}(p)$  the “C-ROC relative to baseline  $b(u)$ ” as the ROC curve with false positive rate

$$\widehat{FP}_b(t) = \frac{\int_W \mathbf{1}\{Z(u) > t\} b(u) du}{\int_W b(u) du}. \quad (54)$$

and unchanged true positive rate (22). This means that  $1 - \widehat{FP}_b(t)$  is the c.d.f. of the covariate value at a randomly selected location with nonuniform probability density proportional to  $b(u)$ . In the context of disease data, the horizontal axis is the “cumulative fraction of susceptibles” rather than the “cumulative fraction of the survey area”. Note that this only depends on  $b(u)/\int_W b(v) dv$ , so it is invariant under rescaling of the baseline. To illustrate the point, consider the mucosa data shown in Figure 2 in Section 3.3. We treat the ECL cells as the cases of interest and we can use the kernel estimate of the intensity of non-ECL cells shown in the left panel of Figure 20 as the baseline proportional to the reference population density. The right panel of Figure 20 shows  $R_{Z,x,b}^<$ , where  $Z$  is distance to

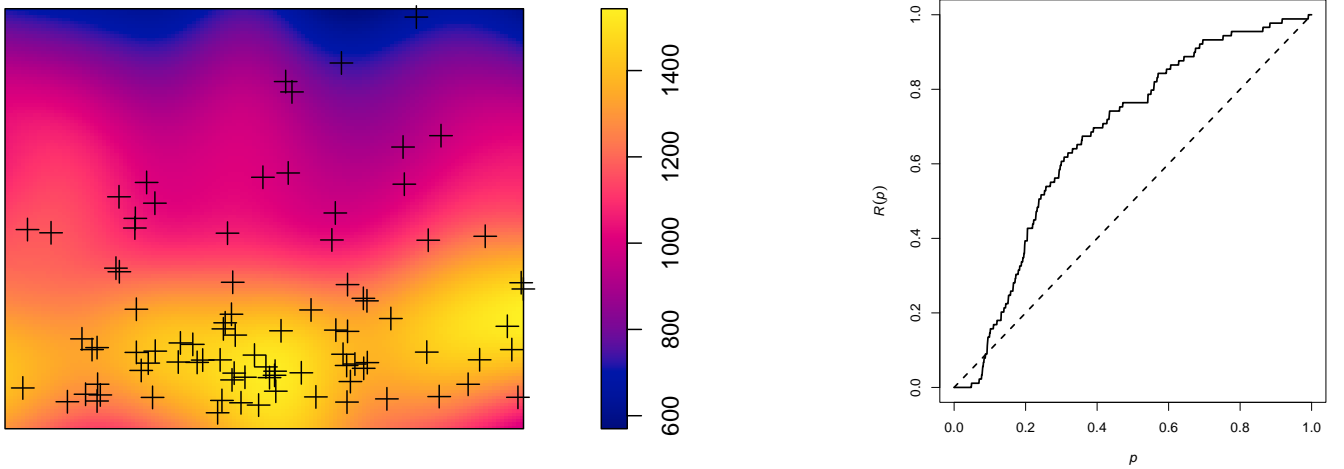


Figure 20: Analysis of gastric mucosa data of Figure 2 using baseline-adjusted C-ROC. *Left:* Kernel density estimate of intensity of non-ECL cells; ECL cells overlaid as black crosses. *Right:* Baseline-adjusted C-ROC curve for distance to the stomach wall ( $y$ -coordinate) treating short distances as favorable for ECL cells, and using the intensity estimate of non-ECL cells as baseline.

stomach wall ( $y$ -coordinate),  $x$  is the pattern of ECL cells, and  $b(u)$  is the kernel density estimate of the intensity of non-ECL cells. It clearly shows that (apart from very short distances) ECL cells appear closer to the stomach wall than cells in general. Another way to think about this example is that the baseline  $b(u)$  appears as the intensity of a reference model, which stipulates that the intensity of ECL cells is proportional to the kernel density estimate of the intensity of non-ECL cells (or any parametric model for this intensity for that matter). In general terms when  $b(u)$  is the intensity of a reference model the interpretation of the horizontal axis of the ROC curve is “cumulative fraction of cases/deposits/events predicted to be captured by reference model”. Other appropriate examples of the baseline  $b(u)$  include (1) the Jacobian of the spatial coordinate system (so the horizontal axis is ‘cumulative fraction of true area’); (2) the spatially-varying cost of exploration (so the horizontal axis is ‘cumulative fraction of total cost of exploration’); and (3) the micro-scale percentage of area that is habitable or usable, for example the spatially-varying fraction of area occupied by small patches of dry land in a swamp (so the horizontal axis is ‘cumulative fraction of habitable area’).

The baseline could also be the fitted intensity of a model that does not involve the covariate  $Z$ . This idea is explored further in Section 8.4 below.

For pixel data as in Section 4.1.1 we can make an analogous definition of the ROC relative to baseline weights  $b_j \geq 0$ , for each pixel  $Q_j$ . Define the baseline-adjusted false positive rate by

$$\widehat{FP}_b(t) = \frac{\sum_{j=1}^J b_j (1 - y_j) \hat{y}_j}{\sum_{j=1}^J b_j (1 - y_j)}, \quad (55)$$

where, as before,  $y_j$  is the presence-absence indicator and  $\hat{y}_j = \mathbf{1}\{z_j > t\}$  is the classifier. Combining this with the usual empirical true positive rate  $\widehat{TP}(t)$  from (18) yields the C-ROC curve  $R_{Z,y,b}$  where  $\mathbf{b} = (b_1, \dots, b_J)$  is the vector

of baseline weights for each pixel. In the same way any of the other definitions of ROC curves (M-ROC, model-predicted ROC curves, ...) can be relative to a baseline by introducing pixel weights or a weight function in the definition of the false positive rate.

#### 8.4 Partial ROC curve for dropping or adding an explanatory variable

When we have fitted a model involving several covariates, we can construct an array of plots representing the effect of dropping each existing term in the model. Each panel is an ROC plot for the covariate in question, with the baseline being the fitted intensity when this covariate is removed. An ROC curve lying close to the diagonal line suggests that the covariate can be dropped from the model. This is analogous to a partial residual plot, so we shall call it the *partial ROC*, and the associated AUC value is the *partial AUC*.

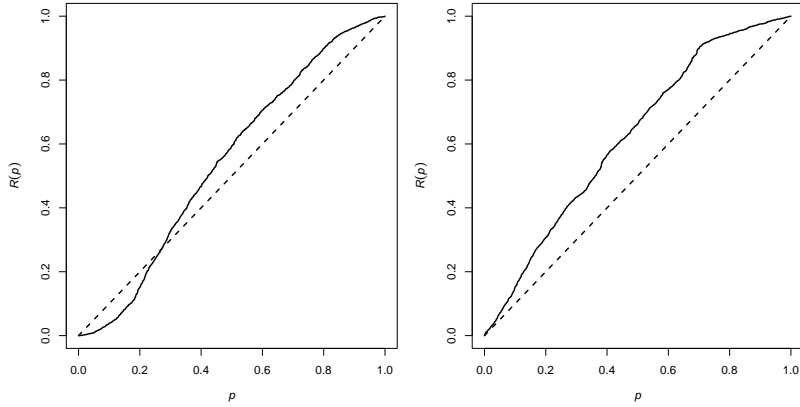


Figure 21: Partial ROC curves for dropping covariates from a fitted model. Poisson point process, additive loglinear model for the *Beilschmiedia* data involving the covariates Elevation and Gradient. *Left*: ROC curve for dropping Elevation. *Right*: ROC curve for dropping Gradient.

Figure 21 shows the partial ROC curves for dropping the Elevation and Gradient variables, respectively, from the additive loglinear Poisson model for the *Beilschmiedia* data (treating large values as favorable to trees, in both panels). It suggests that the Elevation variable could be dropped without compromising the model. corresponding partial AUC values are 0.54 for elevation and 0.62 for slope. These plots are visually very similar to the C-ROC plots with constant baseline; maximum discrepancies are 0.072 for elevation, 0.026 for slope.

Similarly, given a fitted model and a list of covariates which were *not* included in the fitted model, we can construct an array of ROC plots representing the effect of *adding* each one of the additional covariates to the fitted model. For each curve, the baseline is the intensity of the *original* fitted model. A partial ROC curve lying close to the diagonal line suggests that the covariate does not improve the ranking ability of the fitted model and should not be added to the model.

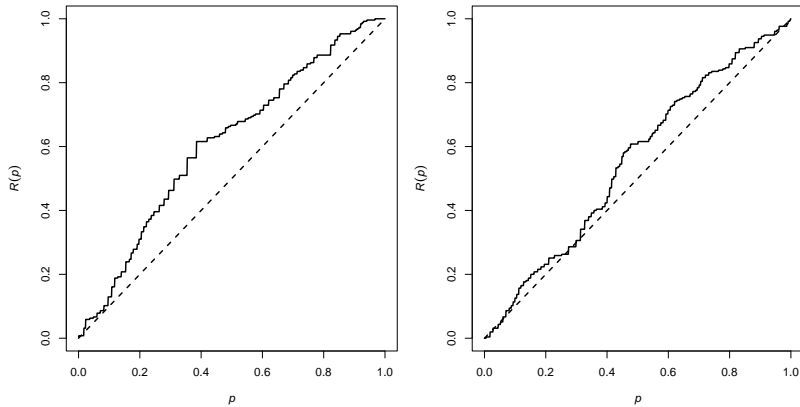


Figure 22: Partial ROC curves for adding covariates to a fitted model. Poisson point process, additive loglinear model for the Murchison gold data involving greenstone indicator and distance to nearest fault. *Left*: ROC curve for adding the *x* coordinate. *Right*: ROC curve for adding the *y* coordinate.

Figure 22 shows the partial ROC curves for adding the  $x$  (Easting) and  $y$  (Northing) coordinates, considered as spatial covariates, to the additive loglinear model for the Murchison data involving both the greenstone indicator and distance to nearest fault. Corresponding partial AUC values are 0.61 and 0.55. The left panel suggests that adding the  $x$  coordinate as a covariate would improve the ranking performance of the model, while the right panel provides only weak support for adding the  $y$  coordinate. Since  $x$  and  $y$  coordinates are always available, plots similar to Figure 22 could be useful as a model diagnostic.

## 9 Model checking using ROC

There are numerous claims that ROC curves can be used for model validation [Nykänen et al., 2015]. Our reading of this literature is that the term “validation” is not being used in the statistical sense: rather, a model is said to be “validated” if its ranking performance is found to be sufficiently high.

It is shown above that the empirical M-ROC does not itself contain diagnostic information about the goodness-of-fit of the model. Instead, the shape of the empirical M-ROC curve is largely indicative of the spatial variation in the fitted model probabilities or intensity function.

Informal model diagnostics are typically based on comparison between observed and predicted values of a statistic. This suggests that a comparison between the empirical and model-predicted ROC curves would enable diagnostic checking of models. This approach could be applied either to C-ROC or M-ROC curves.

For brevity we assume the spatial data are a point pattern  $x$  in continuous space (but similar comments apply in other cases). Suppose a point process model has been fitted to  $x$  yielding fitted intensity function  $\hat{\lambda}$ .

### 9.1 Model checking using C-ROC

First consider C-ROC curves. For any point process model with intensity function  $\lambda(u)$ , the theoretical C-ROC curve  $R_{Z,\lambda}$  for a covariate  $Z$  is based on the theoretical true positive rate (24) and false positive rate (23). For a fitted model with intensity  $\hat{\lambda}(u)$ , the “model-predicted” C-ROC curve  $R_{Z,\hat{\lambda}}$  was defined similarly in Section 4.1.2 by replacing  $\lambda$  by  $\hat{\lambda}$  in (24).

For any spatial covariate  $Z$  we could compare the empirical C-ROC curve  $R_{Z,x}$  and the model-predicted C-ROC curve  $R_{Z,\hat{\lambda}}$ . If the model is correct, with true intensity  $\lambda$ , then under suitable conditions under a large sample regime, both the functions  $R_{Z,x}$  and  $R_{Z,\hat{\lambda}}$  converge to  $R_{Z,\lambda}$  as distribution functions (i.e. pointwise at every continuity point of  $R_{Z,\lambda}$ ). Hence the discrepancy between the empirical C-ROC and model-predicted C-ROC should be small.

If the model is misspecified, and the true process has intensity  $\lambda^\#$ , then under suitable conditions  $R_{Z,x}$  converges to  $R_{Z,\lambda^\#}$  but  $R_{Z,\hat{\lambda}}$  converges to  $R_{Z,\lambda^*}$ , where  $\lambda^*$  is determined by the behaviour of the model-fitting procedure applied to the true point process. A discrepancy between the empirical and model-predicted C-ROC curves suggests that the model is misspecified.

This technique can be applied to any covariate  $Z$ , whether or not the model involves  $Z$ . It may be useful for detecting departures from the model due to effects that are not included in the model.

Figure 23 shows two applications of this diagnostic to the Murchison data. The fitted model is a Poisson point process in which log intensity is an additive linear function of distance to nearest fault and greenstone indicator. The left panel of Figure 23 shows the empirical C-ROC and the model-predicted C-ROC for the distance to nearest fault, suggesting a good fit. The right panel shows the empirical C-ROC and model-predicted C-ROC for the  $x$  (Easting) coordinate. This plot suggests that this model does not capture the fact that mineral deposits are relatively more frequent on the eastern side of the study region.

### 9.2 Model checking using M-ROC

An alternative technique is to compare the empirical M-ROC  $R_{\hat{\lambda},x}$  and the model-predicted M-ROC  $R_{\hat{\lambda},\hat{\lambda}}$  for a fitted model. If the model is true then under suitable conditions these two curves both converge to the theoretical M-ROC  $R_{\lambda,\lambda}$  for the model. As shown in Lemma 11, this limiting curve is concave. If the model is misspecified then (with the same notation as above)  $R_{\hat{\lambda},x} \rightarrow R_{\lambda^*,\lambda^\#}$  while  $R_{\hat{\lambda},\hat{\lambda}} \rightarrow R_{\lambda^*,\lambda^*}$  so that there is a nonzero discrepancy, and the empirical M-ROC may converge to a function which is not concave. Deviation between the two curves, or non-convex shape, suggests that the model is not correct.

Figure 24 shows the M-ROC curve  $R_{\hat{\lambda},x}(p)$  (solid lines) and model-predicted M-ROC curve  $R_{\hat{\lambda},\hat{\lambda}}(p)$  (dashed lines) for the Poisson model in which log intensity is a linear function of distance to nearest fault and the greenstone indicator. This suggests a good fit.

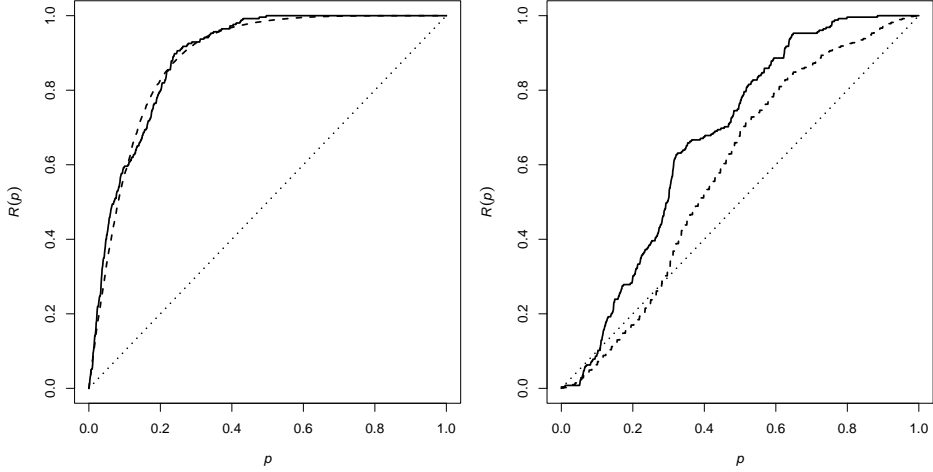


Figure 23: Diagnostics using C-ROC. Model fitted to the Murchison data in which log intensity is an additive linear function of distance to nearest fault and of greenstone indicator. *Left*: Empirical C-ROC curve  $R_{Z,x}$  (solid lines) for the distance-to-nearest-fault covariate  $Z$  in the Murchison data, and predicted C-ROC curve  $R_{Z,\hat{\lambda}}(p)$  (dashed lines) for the same covariate, suggesting a good fit. *Right*: Empirical C-ROC curve  $R_{Z,x}(p)$  (solid lines) and model-predicted C-ROC curve  $R_{Z,\hat{\lambda}}(p)$  (dashed lines) for the Murchison gold data, where the covariate  $Z$  is the  $x$  (Easting) coordinate, suggesting a mediocre fit.

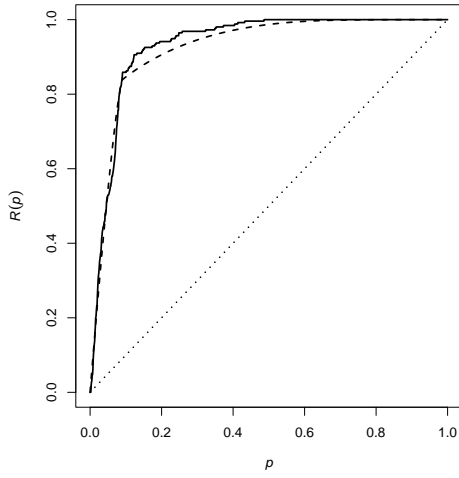


Figure 24: Empirical M-ROC curve  $R_{\hat{\lambda},x}(p)$  (solid lines) and model-predicted M-ROC curve  $R_{\hat{\lambda},\hat{\lambda}}(p)$  (dashed lines) for the Poisson model of the Murchison gold deposits, in which log intensity is a linear function of distance to nearest fault and greenstone indicator.

These diagnostic tools may be useful for detecting departures from a fitted model. Their weaknesses are the same as those described above for ROC curves in general. For example, suppose that the model is correct except for misspecification by an increasing transformation. That is, the true process has intensity  $\lambda_0(u)$  while the intensity of the model is  $\lambda(u) = \psi(\lambda_0(u))$  where  $\psi$  is an increasing transformation, possibly depending on parameters of the model. Then the ROC is the same as if the model were completely correct:  $R_{\psi \circ \lambda_0, \lambda_0}(p) \equiv R_{\lambda_0, \lambda_0}(p)$  and when the law of large numbers is a good approximation,  $R_{\hat{\lambda},x}(p) \equiv R_{\lambda_0, \lambda_0}$ . Comparison of the empirical and model-predicted C-ROC curves cannot distinguish this kind of misspecified model from the correct model. Perfect agreement between  $R_{\hat{\lambda},x}(p)$  and  $R_{\hat{\lambda},\hat{\lambda}}(p)$  does not prove the model is correct.

## 10 Discussion

### 10.1 Summary of main findings

This article has four main findings. First, we have established that the current use of ROC curves to evaluate model performance is partly erroneous. Second, the correct interpretation of ROC curves has been found by elucidating their connection to other statistical tools. Third, we have emphasised that there are many versions of the ROC curve, and have proposed new ROC curves for spatial data, allowing better interpretation and expanding the scope of application. Fourth, we have proposed new practical techniques for valid evaluation of model performance by comparing empirical and fitted ROC curves.

The first finding concerns the correct interpretation of ROC curves for a fitted model. In the applications literature, “the” ROC curve for a species distribution model is understood to mean the ROC curve based on the fitted presence probabilities under the model (Section 5). We call this the “M-ROC”. We find that the M-ROC is invariant under monotone transformation of model predictions (probabilities or intensities) (Section 5.4.1). This implies that the M-ROC cannot distinguish between two models based on the same covariate (if both models are based only on that covariate, and are both monotone). If a model involves only one covariate, then the M-ROC collapses to the C-ROC, a curve constructed without reference to the model (Section 5.4.2) and therefore has nothing to do with the goodness-of-fit of the model. We demonstrated that ROC or AUC is not a measure of goodness-of-fit of a fitted model (Section 5.4.3); rather, it is a measure of “badness-of-fit” of the null model. The use of ROC in this context contravenes the standard practice that a test of goodness-of-fit should be based on a covariate that was not included in the model. The M-ROC is a measure of “ranking ability” rather than “predictive power”. The M-ROC is completely bound to the study region (Sections 4.5.1 and 5.4.4), mostly because of inhomogeneity in the study region. It is not possible to extrapolate the ROC from one region to another; restriction to a sub-region can lead to Simpson’s paradox; restriction to a more homogeneous sub-region lowers the AUC; ROC cannot be used to predict the response to changes in the covariate value (such as climate change). ROC and AUC are also insensitive to dependence on other covariates not included in the model (Section 6.3).

The second finding concerns the connections between ROC curves and other statistical tools, in the context of spatial data. It is well known that ROC curves are closely related to P-P plots and other tools for distributional comparison. In the case of a single covariate, we show that the AUC and Youden index are related to the Berman-Waller-Lawson test and Kolmogorov-Smirnov test, respectively, of the null hypothesis of uniformity (Section 6). That is, they are measures of the degree of departure from the null model, rather than measures of agreement with the fitted model. We also established connections between ROC curves and the function  $\rho$  (the resource selection function or prospectivity index) which expresses the presence probability or intensity as a function of the covariate (Section 7). The function  $\rho$  can be interpreted as a law or model predicting the probability of occurrence as a function of the covariates, in a form which could be extrapolated from one region to another, while the ROC cannot. These connections provide insight and implies that these different techniques are not independent pieces of evidence.

The third finding concerns different versions of the ROC curve in the context of spatial data. We emphasised that M-ROC is only one particular application of the ROC concept. We argued that there are many ways to apply/define ROC curves in this context other than the M-ROC. We introduced the C-ROC which is based on a covariate rather than a model (Section 4). The C-ROC is invariant under monotone transformation of covariate, and is a measure of “ranking ability” rather than “predictive power”. We introduced predicted (fitted) and theoretical (true) versions of the M-ROC and C-ROC (Sections 5.1.1 and 5.1.2). We extended all these concepts to spatial point pattern data in continuous space (Sections 4.1.2 and 5.1.2). The continuous case is often simpler to understand. We established that the pixel-based ROC converges as pixel size tends to zero; therefore, ROC curves obtained using different pixel sizes are approximately consistent. We note that the ROC for presence-absence data effectively assumes that pixels have equal area; this is sensitive to the choice of coordinate system; calculating ROC on a square grid in latitude-longitude coordinates would be “wrong” or “biased”. We proposed leave-one-out calculation for the M-ROC to avoid overfitting (end of Section 5.1.1). We extended the M-ROC and C-ROC to spatial case-control point pattern data (Sections 4.1.3, 4.3.2, 5.1.3). We proposed more extensions of ROC including the ROC relative to a baseline (Section 8.3), ROC with data weights (Section 8.2), ROC restricted to a subregion (Section 8.1) and especially the partial ROC for dropping an explanatory variable from a fitted model or for adding an explanatory variable to the model (Section 8.4).

The fourth finding is a set of new proposed practical techniques for valid evaluation of model performance by comparing empirical and fitted ROC curves. The shape of the empirical C-ROC carries diagnostic information about whether a monotone model is appropriate (hence whether ROC analysis is appropriate) (Section 9). The theoretical and model-predicted M-ROC are always concave. (Corollary 1 and Lemma 11 in Section 7.2). The theoretical M-ROC is the most optimistic of all theoretical ROC curves (Section 5.4.6). Model validation is possible by comparing empirical and predicted ROC curves (either C-ROC or M-ROC) (Section 9). C-ROC has potential as a tool for variable

selection (since it is insensitive to monotone transformations of the explanatory variable). We also defined partial ROC curves for evaluating the effect of adding another explanatory variable to an existing model, or the effect of removing one of the explanatory variables from the model. The dependence of ROC curves on the study region can be turned to advantage, for example to consider sub-populations or to understand “interaction” between variables.

## 10.2 Discussion of findings

The most important implication of this study is that ROC curves for spatial data should not be treated as providing confirmation of the validity or goodness-of-fit of a model. They measure the ranking ability of the model, within the study region. The ROC is bound to the choice of study region. There is no ability to extrapolate or interpolate the ROC from one region to another. There is no ability to predict response to changes in the values of predictor variables, such as response to climate change. The ROC curve is also insensitive to detecting effects that only involve a small fraction of the population (see Appendix D).

On the other hand, the ROC has advantages for *exploratory* data analysis. The insensitivity of the ROC to monotone transformations can be exploited for variable selection. It is an advantage that the ROC can be used before committing to a particular parametric form of model (for selecting variables, for deciding whether a monotone model is appropriate, etc.). Dependence on the study region can be an advantage when the objective is to segregate a specific region, e.g. to find the best place to put a wind farm to avoid harm to birds. The ROC is useful for gauging the magnitude of the “effect” of a covariate in a particular spatial region, whereas a statistical model is a general relationship which could have either a large or small effect in different regions.

Our study presents several new practical opportunities involving ROC curves. We proposed a technique for model checking by comparing model-predicted and empirical versions of ROC. The shape of the ROC curve is diagnostic: if the ROC curve is concave/convex, a monotone model is appropriate, and the approach is valid. (Note the model-predicted ROC is always concave.)

### 10.2.1 Questions for future research

It would be useful to obtain expressions for the variance of the M-ROC for specific models fitted by maximum likelihood, especially for logistic regression and for the loglinear Poisson point process.

Since ROC curves are closely related to P-P plots (Section 2.4), it may be useful to construct **Q-Q plots** for the same data, as these frequently contain complementary information [Wilk and Gnanadesikan, 1968].

**Acknowledgements** We thank Professor Matt Wand for insightful comments, and Andrew Hardegen, Kassel Hingee and Tom Lawrence who participated in our early research on this topic.

The Murchison data (Figure 4) are reproduced by permission of Dr Tim Griffin of the Geological Survey of Western Australia and by Dr Carl Knox-Robinson. These data are publicly available in the R package `spatstat` [Baddeley et al., 2015]. Gold deposit and occurrence locations were obtained from a database compiled by the Geological Survey of Western Australia [Geological Survey of Western Australia, 1994]; they include deposits of all sizes and are based on map surveys at a scale of 1:50,000 or better [Knox-Robinson and Groves, 1997]. Fault locations were compiled by Watkins and Hickman [1990]. These data were presented and analysed by Knox-Robinson and Groves [1997] and subsequently by Groves et al. [2000], Foxall and Baddeley [2002], Baddeley et al. [2015], Baddeley [2018]. Although there exist more up-to-date versions of this survey, we use the original 1994 version to allow comparison between different published analyses of the same data.

This project was partially funded by *The Royal Society of New Zealand* through Marsden Grant 23-UOO-148.

## References

F.P. Agterberg. Automatic contouring of geological maps to detect target areas for mineral exploration. *Journal of the International Association for Mathematical Geology*, 6:373–395, 1974.

N. Altman and C. Leger. Bandwidth selection for kernel distribution function estimation. *Journal of Statistical Planning and Inference*, 46:195–214, 1995.

T.W. Anderson and D.A. Darling. Asymptotic theory of certain ‘goodness-of-fit’ criteria based on stochastic processes. *Annals of Mathematical Statistics*, 23:193–212, 1952.

T.W. Anderson and D.A. Darling. A test of goodness of fit. *Journal of the American Statistical Association*, 49:765–769, 1954.

M. Austin. Species distribution models and ecological theory: a critical assessment and some possible new approaches. *Ecological Modelling*, 200:1–19, 2007.

A. Baddeley. A statistical commentary on mineral prospectivity analysis. In B.S. Daya Sagar, Q. Cheng, and F.P. Agterberg, editors, *Handbook of Mathematical Geosciences: Fifty Years of IAMG*, chapter 2, pages 25–65. International Association for Mathematical Geosciences, 2018.

A. Baddeley and R. Turner. Spatstat: an R package for analyzing spatial point patterns. *Journal of Statistical Software*, 12(6):1–42, 2005. URL: [www.jstatsoft.org](http://www.jstatsoft.org), ISSN: 1548-7660.

A. Baddeley, R. Turner, J. Møller, and M. Hazelton. Residual analysis for spatial point processes (with discussion). *Journal of the Royal Statistical Society, Series B*, 67(5):617–666, 2005.

A. Baddeley, M. Berman, N.I. Fisher, A. Hardegen, R.K. Milne, D. Schuhmacher, R. Shah, and R. Turner. Spatial logistic regression and change-of-support for Poisson point processes. *Electronic Journal of Statistics*, 4:1151–1201, 2010. doi: 10.1214/10-EJS581.

A. Baddeley, Y.M. Chang, Y. Song, and R. Turner. Nonparametric estimation of the dependence of a spatial point process on a spatial covariate. *Statistics and its Interface*, 5:221–236, 2012.

A. Baddeley, E. Rubak, and R. Turner. *Spatial Point Patterns: Methodology and Applications with R*. Chapman and Hall/CRC, London, 2015. ISBN 9781482210200.

A. Baddeley, W. Brown, R.K. Milne, G. Nair, S. Rakshit, T. Lawrence, A. Phatak, and S.C. Fu. Optimal thresholding of predictors in mineral prospectivity analysis. *Natural Resources Research*, 30:923–969, 2021.

M. Berman. Testing for spatial association between a point process and another stochastic process. *Applied Statistics*, 35:54–62, 1986.

J.F. Bithell. Estimation of relative risk functions. *Statistics in Medicine*, 10:1745–1751, 1991.

G. Bonham-Carter. *Geographic Information Systems for Geoscientists: Modelling with GIS*. Number 13 in Computer Methods in the Geosciences. Pergamon Press / Elsevier, Kidlington, Oxford, UK, 1995.

M.S. Boyce, P.R. Vernier, S.E. Nielsen, and F.K.A. Schmiegelow. Evaluating resource selection functions. *Ecological modelling*, 157:281–300, 2002.

D.R. Brillinger. Comparative aspects of the study of ordinary time series and of point processes. In P.R. Krishnaiah, editor, *Developments in Statistics*, pages 33–133. Academic Press, New York, London, 1978.

E.J.M. Carranza. Data-driven modeling of mineral prospectivity. In M. Hale, editor, *Handbook of Exploration and Environmental Geochemistry 11: Geochemical Anomaly and Mineral Prospectivity Mapping in GIS*, chapter 8, pages 249–310. Elsevier, 2009a.

Emmanuel John M. Carranza. *Geochemical Anomaly and Mineral Prospectivity Mapping in GIS*, volume 11 of *Handbook of Exploration and Environmental Geochemistry*. Elsevier, Amsterdam, the Netherlands, 2009b. URL <https://researchonline.jcu.edu.au/40323/>.

Y. Chen and W. Wu. Isolation forest as an alternative data-driven mineral prospectivity mapping method with a higher data-processing efficiency. *Natural Resources Research*, 28(1):31–46, January 2019.

R. Condit. *Tropical Forest Census Plots*. Springer-Verlag, 1998.

R. Condit, S.P. Hubbell, and R.B. Foster. Changes in tree species abundance in a neotropical forest: impact of climate change. *Journal of Tropical Ecology*, 12:231–256, 1996.

H. Cramér. On the composition of elementary errors: II, Statistical applications. *Skandinavisk Aktuarietidskrift*, 11: 141–180, 1928.

N.A.C. Cressie. *Statistics for Spatial Data*. John Wiley and Sons, New York, 1991.

R.B. D'Agostino and M.A. Stephens. *Goodness-of-Fit Techniques*, volume 68 of *Statistics: Textbooks and Monographs*. Marcel Dekker, New York, 1986.

D.J. Daley and D. Vere-Jones. *An Introduction to the Theory of Point Processes*. Springer-Verlag, New York, 1988.

P.J. Diggle. *Statistical Analysis of Spatial Point Patterns*. Academic Press, London, 1983.

P.J. Diggle. A point process modelling approach to raised incidence of a rare phenomenon in the vicinity of a pre-specified point. *Journal of the Royal Statistical Society, Series A*, 153:349–362, 1990.

P.J. Diggle. *Statistical Analysis of Spatial and Spatio-Temporal Point Patterns*. Chapman and Hall/CRC, Boca Raton, FL, third edition, 2014.

P.J. Diggle and B. Rowlingson. A conditional approach to point process modelling of elevated risk. *Journal of the Royal Statistical Society, Series A*, 157(3):433–440, 1994.

P.J. Diggle, P. Zheng, and P. Durr. Non-parametric estimation of spatial segregation in a multivariate point process: bovine tuberculosis in Cornwall, UK. *Applied Statistics*, 54:645–658, 2005.

P.J. Diggle, V. Gómez-Rubio, P.E. Brown, A.G. Chetwynd, and S. Gooding. Second-order analysis of inhomogeneous spatial point processes using case-control data. *Biometrics*, 63:550–557, 2007.

P. Dixon. Testing spatial segregation using a nearest-neighbour contingency table. *Ecology*, 75(7):1940–1948, 1994.

J.P. Egan. *Signal Detection Theory and ROC Analysis*. Academic Press, New York, 1975.

J. Elith and J. R. Leathwick. Species distribution models: Ecological explanation and prediction across space and time. *Annual Review of Ecology, Evolution, and Systematics*, 40:677–697, 2009.

A.G. Fabbri and C.-J. Chung. On blind tests and spatial prediction models. *Natural Resources Research*, 17(2):107–118, 2008.

A.H. Fielding and J.F. Bell. A review of methods for the assessment of prediction errors in conservation presence/absence models. *Environmental Conservation*, 24:38–49, 1997.

A. Ford, K.J. Peters, G.A. Partington, P.L. Blevin, P.M. Downes, J.A. Fitzherbert, and J.E. Greenfield. Translating expressions of intrusion-related mineral systems into mappable spatial proxies for mineral potential mapping: Case studies from the Southern New England Orogen, Australia. *Ore Geology reviews*, 111(102943), 2019.

R. Foxall and A. Baddeley. Nonparametric measures of association between a spatial point process and a random set, with geological applications. *Applied Statistics*, 51(2):165–182, 2002.

J. Franklin. *Mapping Species Distributions: Spatial Inference and Prediction*. Cambridge University Press, Cambridge, UK, 2009.

Geological Survey of Western Australia. MINEDEX database, 1994. <https://dmp.wa.gov.au/Mines-and-mineral-deposits-1502.aspx>.

A. Goodacre, G.F. Bonham-Carter, F.P. Agterberg, and D.F. Wright. A statistical analysis of the spatial association of seismicity with drainage patterns and magnetic anomalies in western Quebec. *Tectonophysics*, 217:285–305, 1993.

D.I. Groves, R.J. Goldfarb, C.M. Knox-Robinson, J. Ojala, S. Gardoll, G.Y. Yun, and P. Holyland. Late-kinematic timing of orogenic gold deposits and significance for computer-based exploration techniques with emphasis on the Yilgarn Block, Western Australia. *Ore Geology Reviews*, 17:1–38, 2000.

Y. Guan. On consistent nonparametric intensity estimation for inhomogeneous spatial point processes. *Journal of the American Statistical Association*, 103:1238–1247, 2008.

Y. Guan and H. Wang. Sufficient dimension reduction for spatial point processes directed by Gaussian random fields. *Journal of the Royal Statistical Society, Series B*, 72:367–387, 2010.

P. Hall and R.J. Hyndman. An improved method for bandwidth selection when estimating ROC curves. *Statistics and Probability Letters*, 64:181–189, 2003.

P. Hall, R.J. Hyndman, and Y. Fan. Nonparametric confidence intervals for receiver operating characteristic curves. *Biometrika*, 91:743–750, 2004.

D.J. Hand and R.J. Till. A simple generalization of the area under the ROC curve to multiple class classification problems. *Machine Learning*, 45(2):171–186, 2001.

J.A. Hanley and B.J. McNeil. The meaning and use of the area under a receiver operating characteristic (ROC) curve. *Radiology*, 143:29–36, 1982.

M.L. Hazelton and T.M. Davies. Inference based on kernel estimates of the relative risk function in geographical epidemiology. *Biometrical Journal*, 51:98–109, 2009.

A. H. Hirzel, V. Le Lay, V. Helfer, C. Randin, and A. Guisan. Evaluating the ability of habitat suitability models to predict species presences. *Ecological Modelling*, 199:142–152, 2006.

S.P. Hubbell and R.B. Foster. Diversity of canopy trees in a neotropical forest and implications for conservation. In S.L. Sutton, T.C. Whitmore, and A.C. Chadwick, editors, *Tropical Rain Forest: Ecology and Management*, pages 25–41. Blackwell Scientific Publications, Oxford, 1983.

J. Illian, A. Penttinen, H. Stoyan, and D. Stoyan. *Statistical Analysis and Modelling of Spatial Point Patterns*. John Wiley and Sons, Chichester, 2008.

M.F. Jarner, P.J. Diggle, and M.G. Chetwynd. Estimation of spatial variation in risk using matched case-control data. *Biometrical Journal*, 44:936–945, 2002.

A. Jiménez-Valverde. Insights into the area under the receiver operating characteristic curve (AUC) as a discrimination measure in species distribution modelling. *Global Ecology and Biogeography*, 21:498–507, 2012.

M. Khademi Zahedi. *Linking geophysics and geology through borehole data: a framework for quantifying the value of information in mineral exploration*. PhD thesis, University of South Australia, 2025.

C.M. Knox-Robinson and D.I. Groves. Gold prospectivity mapping using a geographic information system (GIS), with examples from the Yilgarn Block of Western Australia. *Chronique de la Recherche Minière*, 529:127–138, 1997.

A. Kolmogorov. Sulla determinazione empirica di una legge di distribuzione. *Giornale dell'Istituto Italiano degli Attuari*, 4:83–91, 1933.

W.J. Krzanowski and D.J. Hand. *ROC Curves for Continuous Data*. Chapman and Hall/CRC Press, London/Boca Raton, 2009.

K.L. Kvamme. Computer processing techniques for regional modeling of archaeological site locations. *Advances in Computer Archaeology*, 1:26–52, 1983.

K.L. Kvamme. There and back again: revisiting archeological locational modeling. In M.W. Mehrer and K.L. Wescott, editors, *GIS and Archaeological Site Modelling*, pages 3–40. CRC Press, 2006.

A.B. Lawson. On the analysis of mortality events around a prespecified fixed point. *Journal of the Royal Statistical Society, Series A*, 156(3):363–377, 1993.

P.A.W. Lewis. Recent results in the statistical analysis of univariate point processes. In P.A.W. Lewis, editor, *Stochastic Point Processes*, pages 1–54. John Wiley and Sons, New York, 1972.

C.J. Lloyd. The use of smoothed ROC curves to summarise and compare diagnostic systems. *Journal of the American Statistical Association*, 93:1356–1364, 1998.

J.M. Lobo, A. Jiménez-Valverde, and R. Real. AUC: a misleading measure of the performance of predictive distribution models. *Global Ecology and Biogeography*, 17(2):145–151, 2007.

M.O. Lorenz. Methods of measuring the concentration of wealth. *Publications of the American Statistical Association*, 9 (70):209–219, 1905.

S. Manel, H.C. Williams, and S.J. Ormerod. Evaluating presence-absence models in ecology: the need to account for presence. *Journal of Applied Ecology*, 38:921–931, 2001.

B.J.F. Manly, L.L. McDonald, and D.L. Thomas. *Resource Selection by Animals: Statistical Design and Analysis for Field Studies*. Chapman and Hall, London, 1993.

J. Møller and R.P. Waagepetersen. *Statistical Inference and Simulation for Spatial Point Processes*. Chapman and Hall/CRC, Boca Raton, FL, 2004.

B.-H. Nam and R. D'Agostino. Discrimination index, the area under the ROC curve. In C. Huber-Carol, N. Balakrishnan, M.S. Nikulin, and M. Mesbah, editors, *Goodness-of-Fit Tests and Model Validity*, pages 267–279. Birkhäuser, Basel, 2002.

V. Nykänen, I. Lahti, T. Niiranen, and K. Korhonen. Receiver operating characteristics (ROC) as validation tool for prospectivity models — A magmatic Ni–Cu case study from the Central Lapland Greenstone Belt, Northern Finland. *Ore Geology Reviews*, 71:853–860, 2015.

M.S. Pepe. *The Statistical Evaluation of Medical Tests for Classification and Prediction*. Oxford University Press, Oxford, 2003.

A. Porwal, I. Gonzalez-Alvarez, V. Markwitz, T.C. McCuaig, and A. Mamuse. Weights-of-evidence and logistic regression modeling of magmatic nickel sulfide prospectivity in the Yilgarn Craton, Western Australia. *Ore Geology Reviews*, 38(3):184–196, 2010.

T.R.C. Read and N.A.C. Cressie. *Goodness-of-Fit Statistics for Multivariate Data*. Springer-Verlag, New York, 1988.

B.D. Ripley. *Spatial Statistics*. John Wiley and Sons, New York, 1981.

M.D. Ruopp, N.J. Perkins, B.W. Whitcomb, and E.F. Schisterman. Youden index and optimal cut-point estimated from observations affected by a lower limit of detection. *Biometrical journal*, 50(3):419–430, June 2008.

T.W. Sager. Nonparametric maximum likelihood estimation of spatial patterns. *Annals of Statistics*, 10:1125–1136, 1982.

B.W. Silverman. *Density Estimation for Statistics and Data Analysis*. Chapman and Hall, London, 1986.

E. H. Simpson. The interpretation of interaction in contingency tables. *Journal of the Royal Statistical Society, Series B*, 13:238–241, 1951.

N. Smirnov. Table for estimating the goodness of fit of empirical distributions. *Annals of Mathematical Statistics*, 19: 279–281, 1948.

J.W. Tukey. Discussion of paper by F.P. Agterberg and S.C. Robinson. *Bulletin of the International Statistical Institute*, 44(1):596, 1972. Proceedings, 38th Congress, International Statistical Institute.

R. Turner. Point patterns of forest fire locations. *Environmental and Ecological Statistics*, 16:197–223, 2009.

R. von Mises. *Wahrscheinlichkeitsrechnung und Ihre Anwendung in der Statistik und Theoretischen Physik*. Deuticke, Leipzig, 1931.

L. Waller, B. Turnbull, L.C. Clark, and P. Nasca. Chronic disease surveillance and testing of clustering of disease and exposure: Application to leukaemia incidence and TCE-contaminated dumpsites in upstate New York. *Environmetrics*, 3:281–300, 1992.

D.I. Warton and L.C. Shepherd. Poisson point process models solve the “pseudo-absence problem” for presence-only data in ecology. *Annals of Applied Statistics*, 4:1383–1402, 2010.

K.P. Watkins and A.H. Hickman. Geological evolution and mineralization of the Murchison Province, Western Australia. Bulletin 137, Geological Survey of Western Australia, 1990. Published by Department of Mines, Western Australia, 1990. Available online from Department of Industry and Resources, State Government of Western Australia, [www.doir.wa.gov.au](http://www.doir.wa.gov.au).

M.B. Wilk and R. Gnanadesikan. Probability plotting methods for the analysis of data. *Biometrika*, 55:1–17, 1968.

C.M. Yeomans. *Enhancing the Geological Understanding of Southwest England using Machine Learning Algorithms*. PhD thesis, Camborne School of Mines, December 2018.

W.J. Youden. Index for rating diagnostic tests. *Cancer*, 3:32–35, 1950.

G. H. Yule. Notes on the theory of association of attributes in Statistics. *Biometrika*, 2:121–134, 1903.

N. Zhang and K. Zhou. Mineral prospectivity mapping with weights of evidence and fuzzy logic methods. *Journal of Intelligent and Fuzzy Systems*, 29(6):2639–2651, 2015.

K.H. Zou and W.J. Hall. Two transformation models for estimating an (ROC) curve derived from continuous data. *Journal of Applied Statistics*, 27:621–631, 2000.

K.H. Zou, W.J. Hall, and D.E. Shapiro. Smooth nonparametric receiver operating characteristic (ROC) curves for continuous diagnostic tests. *Statistics in Medicine*, 16:2143–2156, 1997.

## APPENDICES

### A ROC curves for subregions

If a region  $W$  has been divided into disjoint subsets  $W_1, W_2$  and results in ROC curves  $R_1(p), R_2(p)$ , then the ROC curve for the entire region  $W$  can be reconstructed only if we also know the areas  $a_i = |W_i|$ , the numbers of data points  $n_i = n(\mathbf{x} \cap W_i)$  in each subregion, and the spatial cumulative distribution functions of the covariate in each subregion,  $F_i(z) = |\{u \in W_i : Z(u) \leq z\}|/|W_i|$ . Then

$$R(p) = \frac{n_1}{n_1 + n_2} R_1(F_1(F^{-1}(p))) + \frac{n_2}{n_1 + n_2} R_2(F_2(F^{-1}(p))), \quad (56)$$

where

$$F(z) = \frac{a_1}{a_1 + a_2} F_1(z) + \frac{a_2}{a_1 + a_2} F_2(z). \quad (57)$$

## B Models for *Beilschmiedia pendula* trees

As a complement to Figure 12 in Section 5.2, the left column of Figure 25 shows contours of the fitted probabilities of the presence of *Beilschmiedia pendula* in 10-metre pixels, for logistic regression models depending on terrain elevation, terrain slope, and elevation and slope together. The right column shows contours of the fitted intensity for loglinear Poisson point process models, depending on terrain elevation, terrain slope, and elevation and slope together.

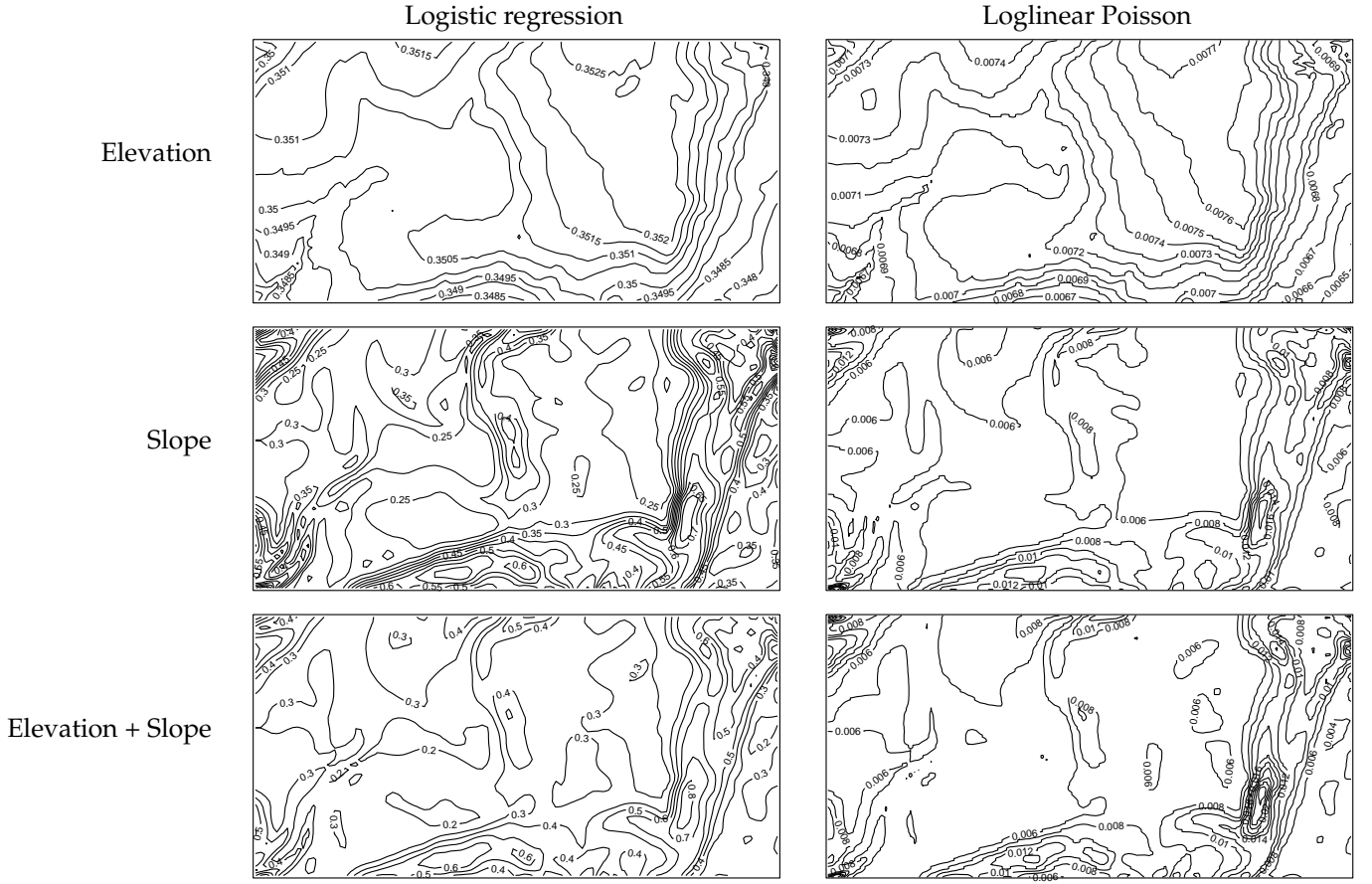


Figure 25: Models in which the *Beilschmiedia* presence probability depends on terrain elevation and/or slope. *Left column* shows contours of fitted probability of presence,  $p$ , within each 10-metre pixel, for logistic regression models. *Right column* shows contours of fitted point process intensity  $\lambda(x)$  for loglinear Poisson models. *Top row*: models depending on terrain elevation. *Middle row*: models depending on terrain slope. *Bottom row*: additive models depending on terrain elevation and slope.

## C Weighted ROC for New Brunswick fires

The left panel of Figure 26 shows the locations of 7108 fires detected in the Canadian province of New Brunswick over a 16-year period [Turner, 2009]. The provincial boundary is classified into coastline and administrative boundary segments. Information available about each fire includes its final size in hectares. Fire size distribution is strongly skewed to the right, with range 0 to 4871 hectares, median 0.1 and mean 3.6. The right panel of Figure 26 shows a contour plot of a kernel-smoothed spatial average of the fire sizes, using the Naradaya-Watson smoother based on an isotropic Gaussian kernel with standard deviation 30 kilometres.

Figure 27 shows unweighted and weighted ROC curves for the New Brunswick fire locations against distance to the coastline, assuming short distances are more favorable to fires. Thin solid lines show the unweighted ROC. Dashed lines show the weighted ROC, with weights equal to fire size. Solid lines show the weighted ROC with weights equal to fire size truncated at 100 hectares. In this example, the weighted ROC (dashed lines) is strongly influenced by the contribution from the largest fires.

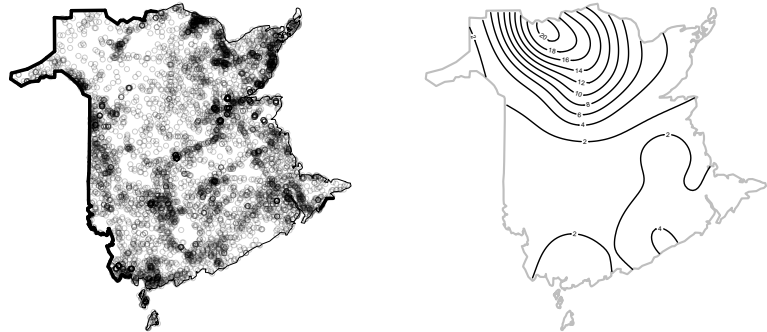


Figure 26: New Brunswick fires. *Left*: fire locations (open circles) and New Brunswick provincial boundary classified into coastline (thin lines) and boundary shared with other territories (thick lines). *Right*: contour plot of kernel-smoothed average size of fires.

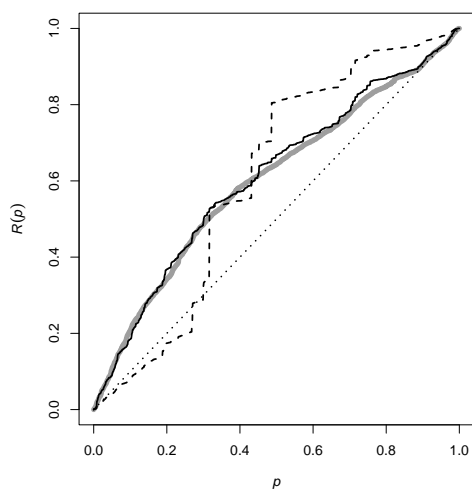


Figure 27: Unweighted and weighted ROC curves for the New Brunswick fire locations against distance to the coastline, assuming short distances are more favorable to fires. Thick grey solid lines: unweighted. Dashed lines: weight is fire size. Thin black solid lines: weight is fire size truncated at 100 hectares.

## D Poor utility of ROC for Chorley-Ribble cancer data

Figure 28 shows the Chorley-Ribble cancer data of Diggle [1990] giving the residential locations of new cases of cancer of the larynx (58 cases) and cancer of the lung (978 cases) in the Chorley and South Ribble Health Authority of Lancashire, England, between 1974 and 1983. The location of a disused industrial incinerator is also given. The aim is to assess evidence for an increase in the incidence of laryngeal cancer close to the incinerator. The lung cancer cases serve as a surrogate for the spatially varying density of the susceptible population. Data analysis in Diggle [1990], Diggle and Rowlingson [1994], Baddeley et al. [2005], Hazelton and Davies [2009] concluded there is significant evidence of an incinerator effect.

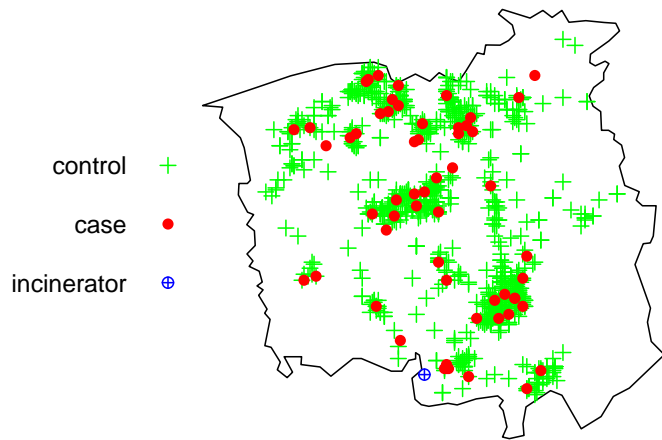


Figure 28: Chorley-Ribble data. Spatial locations of cases of cancer of the larynx (●) and cancer of the lung (+) and a disused industrial incinerator (⊕). Survey area about 25 kilometres across.

Figure 29 shows the C-ROC of distance to incinerator for cases (larynx cancer) against controls (lung cancer) in the Chorley-Ribble data. The corresponding AUC is 0.54. These suggest no evidence against the null hypothesis that distance to incinerator has no effect. The ROC and AUC are not useful in this example, because the incinerator effect causes only a small number of excess cases of larynx cancer.

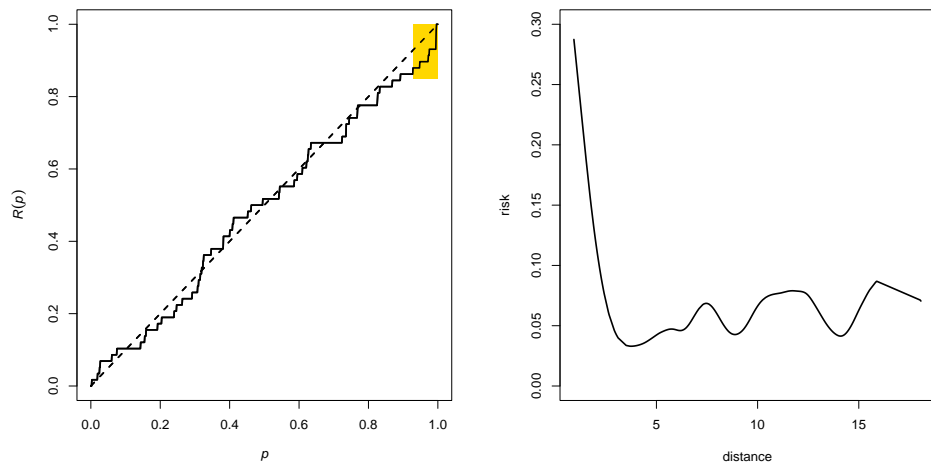


Figure 29: Analysis of the effect of distance to incinerator for the Chorley-Ribble data. *Left*: empirical C-ROC of distance to incinerator. *Right*: spline smoothing estimate of probability of a case as a function of distance to incinerator.

## E Synthetic example of subregion effect

Figure 30 shows a synthetic example in which the original study region is an elongated rectangle  $W = [-10, 10] \times [-1, 1]$  and the point process intensity is  $\lambda(x, y) = 100 \times 2^{-|x|} = \exp(\log 100 - |x| \log 2)$ .

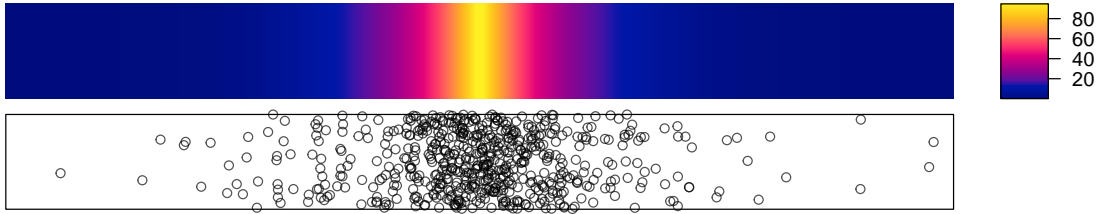


Figure 30: Synthetic example illustrating dependence on study region. *Top*: intensity function. *Bottom*: simulated realisation of Poisson process.

The left panel of Figure 31 shows the empirical C-ROC for the synthetic data in Figure 30 using the absolute value of the  $x$  coordinate as the covariate. Also shown is the theoretical C-ROC curve calculated from (24) and (23). The right panel shows the simulation envelope of C-ROC curves obtained from 50 simulated realisations of the model which produced Figure 30.

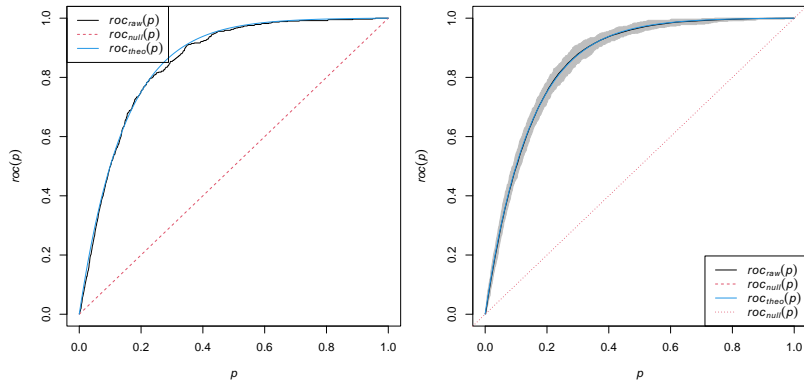


Figure 31: *Left*: empirical C-ROC curve for the simulated point pattern in the bottom panel of Figure 30. *Right*: envelope of C-ROC curves from 50 simulated realisations of the same model.

Figure 32 shows the C-ROC curves derived for different subregions  $[-a, a] \times [-1, 1]$  in the synthetic example. The left panel shows empirical C-ROC curves, and the right panel shows the corresponding theoretical C-ROC curves. The C-ROC curve and AUC value depend greatly on the choice of sub-region.

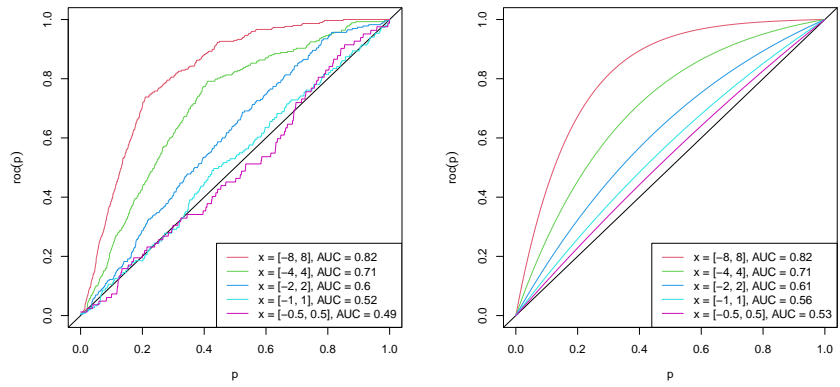


Figure 32: C-ROC curves for the synthetic example in Figure 30 restricted to different sub-regions. *Left*: empirical C-ROC curves for the simulated point pattern in the bottom panel of Figure 30. *Right*: theoretical C-ROC curves for the model with intensity in the upper panel of Figure 30.